Stockholm University

Bachelor Thesis

Degree Project in
Marine Geology 15 hp

Landslides in Lake Orsa, central Sweden

Emelie Ståhl

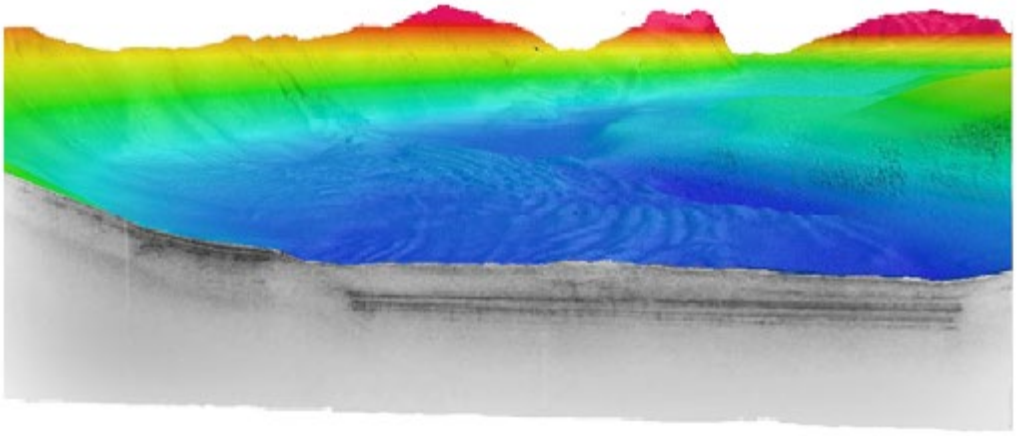

Stockholm 2019

Department of Geological Sciences
Stockholm University
SE-106 91 Stockholm

Abstract

Lake Orsa is situated in the county of Dalarna in central Sweden. The lake is part of the Siljan Ring, which formed approximately 380 Ma by the largest known impact in Europe. The area is of high interest due to its location during the Weichselian deglaciation. The deglacial history in the area is complex, and the behaviour of the receding ice sheet is to some extent not yet fully understood. Submarine landslides were revealed during a geophysical survey, aimed as a site study for a drilling project with the purpose to retrieve an undisturbed sedimentary sequence for studying late- to postglacial evolution in the area. The largest landslide in Lake Orsa mobilized more than 620 000 m^3 of sediment. It has a length of over 630 m and is over 400 m wide. The slides in Lake Orsa are characterized as both confined and emergent submarine landslides. Units with different sedimentological properties have been identified, with a plausible weak horizon in between. The upper unit is believed to prevent up-ward movement of water or gas, possibly leading to overpressure in the lower sediments. The landslides are thought to have occurred during several occasions and seems not to be related to one single event. Plausible causes may be a combination of steep slopes, overpressure zones, and/or low strength horizons in the sub-bottom. The landslides in Lake Orsa have several similarities with the Finneidfjord slide which occurred in northern Norway 1996. The slide was responsible for the loss of four human lives and destroyed nearby houses and a road. Characterizing and understanding submarine landslides are thus an important task to be able to protect citizens as well as infrastructure. Dating the landslides will be possible once the retrieved sediment core during the drilling campaign in one of the slide deposits has been analysed. Relating the slides to the postglacial evolution of the area has proven to be difficult without an age.

Table of Contents

1. Introduction

Lake Orsa is situated in the county of Dalarna in central Sweden. The lake is located between the regional centres Orsa to the northeast, and Mora to the south (Fig. 1). The lake is part of a large Devonian astrobleme, formed approximately 380 Ma (Muhamad et al., 2015). Apart from being part of the well-researched impact structure, the area is also of high interest due to its location during the Late Weichselian deglaciation. The retreating ice-sheet was closely followed by the advancing Ancylus lake (Nordell, 1984). The Ancylus Lake was the predecessor to the Littorina Sea that led into the modern Baltic sea. The Ancylus Lake was named after the discovery of fossils after the fresh-water snail *Ancylus fluviatilis,* indicating that the Lake was in a fresh-water stage (Björck, 1995). The Siljan ring area thus became the borderland between a sub- and supra-aquatic environment. The deglacial history in the area is complicated and the behaviour of the receding ice-sheet is not yet fully understood (Nordell, 1984).

Geophysical mapping with a multibeam echo sounder and a sub-bottom profiler was carried out with Stockholm University´s survey boat *RV Skidbladner* during late summer 2018. This constituted a site study of a drilling project with the aim to retrieve an undisturbed sedimentary sequence for studying the late- to postglacial evolution in the area. The drilling project, led by Per Möller, Lund University, was carried out during the spring 2019. Acquired data reveal several submarine landslides in the sometimes steeply inclined seabed of Lake Orsa. Glacial landforms and other morphological features associated with sedimentary transport and bottom currents are also observed in the acquired data.

Landslides are defined as gravity driven down- and outward movement of slope-forming material caused by shear failure along a surface. Submarine landslides are commonly referred to as “marine”, “submarine” or “subaqueous” in combination with “landslide”, “slope” or “slope failure” (Hampton et al., 1996). The word “submarine” is also commonly used when referring to landslides occurring in lakes and will be used in this report together with “landslide” or just “slide”.

Evidence of submarine landslides are well represented in the geological records, but it is only until the last two decades, thanks to the advances in bathymetric mapping, that their morphology has been properly characterized. Some research examples are work done by Jakobsson et al. (2014) and Mosher et al. (2012) to mention a few. Much of their dynamics and triggering factors are still not well understood, but are often associated with inclined seafloor slopes, high sedimentation rates, fine-grained sediments, and where seafloor rocks are weakened by fractures (Clarke et al., 2012). Local and regional geological conditions and sediment geophysical properties, as well as geomorphology, thus have a large control over slope stability (Vanneste et al., 2012). Their volumes range over several orders of magnitude. The Storegga slide outside the Norwegian coast involved more than 3000 km^3 sediment (Talling et al., 2014). This can be compared with the landslide occurring 1996 in Finneidfjord, northern Norway, which mobilized 0.001 km^3 sediment. Submarine landslides are considered as major geohazards due to their destructive and tsunami-generating potential. The landslide in Finneidfjord encroached 100 – 150 m inland due to its retrogressive behaviour. The landslide destroyed the E6 highway and three houses, and caused the loss of four human lives (L`Heureux et al., 2012). Another example from Norway is the 1978 landslide in Rissa. Rafted blocks and sediments displaced by the landslide generated a tsunami-wave with a run-up height of 6.8 m. Many people were injured, and one person died in this catastrophic event (L`Heureux et al., 2012). They are also responsible for destruction of nearshore and offshore engineering constructions, leading to large economic losses. The need for protection of coastal communities and their citizens, as well as a growing interest in exploiting offshore resources, have contributed to an increased interest for mapping submarine landslides and quantifying the risk they possess (Nadim, 2012). Collecting quantitative data is thus an important step to be able to model the risk they possess, but still a

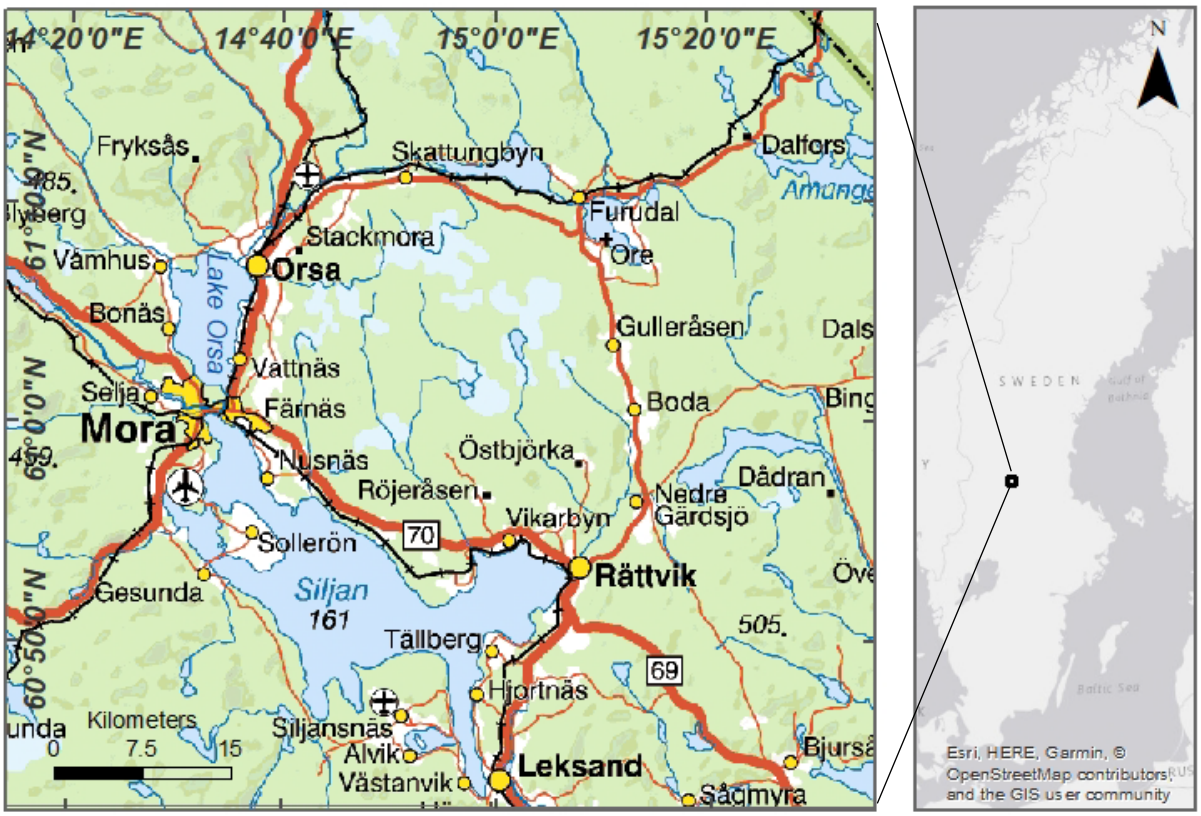

Figure 1: Location map of the Siljan ring area and Lake Orsa, central Sweden. Inset map: GSD Sverigekartan 1:1 miljon, Lantmäteriet. Base map from Esri. Coordinate system SWEREF99 TM. Produced in ArcMap by Emelie Ståhl.

standardized method for data collecting is missing which complicates comparative analysis (Clare et al., 2018).

This project aims to map submarine landslides and glacial features revealed at the bottom of Lake Orsa, with an emphasis on submarine landslides. By analysing the geophysical mapping data, the goals of this project are to characterize the landslides; their overall size, volume, and the displacement of sediment, and by correlating the landslides with other glacial landforms, attempt to relate the landslides to the deglacial and postglacial evolution of the area. The intention is to give answers to; what could have caused these landslides? could the landslides in Lake Orsa have generated a tsunami-wave like the slide in Rissa? and is there any risk for slope failure to occur today?

2. Background

2.1. Physical setting

Lake Orsa has an area of 52.32 km^2 (VISS) and reaches a maximum depth of 94 m (SMHI). The lake has an approximate length of 12 km and a width of around 7 km. Lake Orsa is connected to Lake Siljan through a 4 km long and narrow strait, called Moranoret. The landscape around Lake Orsa is characterized by a typical undulating hilly terrain (Swedish “bergkullsterräng”) and have a general slope towards southeast. The glacial landscape of Ovansiljan (the area north of Lake Siljan) has been thoroughly described by Per Olof Nordell (1984). He speculated that the landscape could be a partial result of selective glacial erosion in weak bedrock zones developed by above described impact. The northwest to southeast trending basins of the more or less parallel river network of Rotälven, Österdalälven, Unnåns, Ämån, Oreälven,

and Vånådalen is thought to have been developed during Silur in connection with the Caledonian orogeny, and is strikingly interrupted by the shape of the completely different Siljan ring valley basin (Nordell, 1984).

2.1.1. Geological setting

Together with Lake Siljan, Lake Ore and Skattungen, Lake Orsa forms the perimeter of the Siljan ring, formed by a large Devonian impact approximately 380.9 +/- 4.6 Ma (Muhamad et al., 2015). The Siljan ring area lies on the boundary between two major geological units of Proterozoic age. Older granitic Svecofennian (~1.9 Ga) rocks dominate to the east, and younger Dala granites of Järna and Siljan types dominate to the west. The Dala granites intruded as part of the Trans-Scandinavian Igneous belt around 1.85 – 1.65 Ga (Henkel&Aro, 2005). Lake Orsa, as part of the western side of the perimeter, is dominated by Dala granites covered by Silurian to Ordovician sedimentary sandstones and limestones. The astrobleme has a central uplift of Svecofennian granite surrounded by a circular depression (Muhamad et al., 2015; Holm-Alwmark et al., 2017). The depression formed by faulting associated with the impact, and the Palaeozoic sedimentary rocks slid downwards. These sedimentary rocks were later preserved from sub-glacial erosion due to their lower and more sheltered location compared to the surrounding rocks (Muhamad et al., 2015). A model from Holm-Alwmark et al. (2017) suggests that the original Palaeozoic sedimentary sequence could have been as thick as 3 km when the meteorite hit the ground, which since then has been exposed to approximately 4 km of erosion (Holm-Alwmark et al., 2017). The sedimentary bedrock is in turn covered by quaternary glacial and glaciofluvial deposits, thereby making bedrock exposures uncommon (Muhamad et al., 2015).

2.1.2. Deglaciation history

The meaning of the word Orsa is believed to originate from the old Swedish word Or, meaning gravel and sand. As the name implies, the region around Orsa is characterized by substantial amounts of gravel and sand deposits, associated with the receding Fennoscandian ice-sheet. Following the last glacial period, the area around Lake Orsa has been subjected to intense glacio-isostatic rebound and a rapid fall of relative sea-level. The deglacial history in the area is complex, and the behaviour of the receding ice-sheet and the exact altitude of the highest coastline have been under intense scientific debate, not least between L. Von Post and B.E. Haldén during the 1930 century. Ice movements inferred from observed striations indicates an older ice movement from NW, a possible main direction in the higher located areas of the landscape from NNW, and a younger ice movement from NE. The ice movements in the thinning ice-sheet was probably increasingly influenced by the local topography (Nordell, 1984).

The Siljan area became deglaciated during the Pre-Boreal, approximately 11,550 to 10,200 cal years BP (Möller, 2005). According to clay-varve studies by Fromm (1991), the Ancylus Lake reached the entrance to Lake Siljan just north of Leksand at varve year 580, which approximately corresponds to year 10,500 – 10,600 cal years BP (Möller, 2005). The receding ice sheet was closely followed by the Ancylus Lake, which gradually inundated the Dalälven river valley and eventually formed Lake Orsa. The deglaciation around Lake Orsa thus took place both above, and below sea-level (Nordell, 1984; Möller, 2005), and the lake sediments bare traces of lacustrine, often varved sediments (Möller, 2005). At the time, the Ancylus Lake had a sea-level approximately between 215 and 220 meter above present sea-level (Nordell, 1984). Due to the topography the area must have been a narrow, and at some places very deep coastal inlet, reaching from Siljan all the way up to Oxberg, and from Lake Orsa stretched out to the area around Lake Ore. The deglaciation environment in Ovansiljan, extensively described by Per Olof Nordell in a number of reports from the nature conservation unit at the county administrative board of Dalarna, constituted the

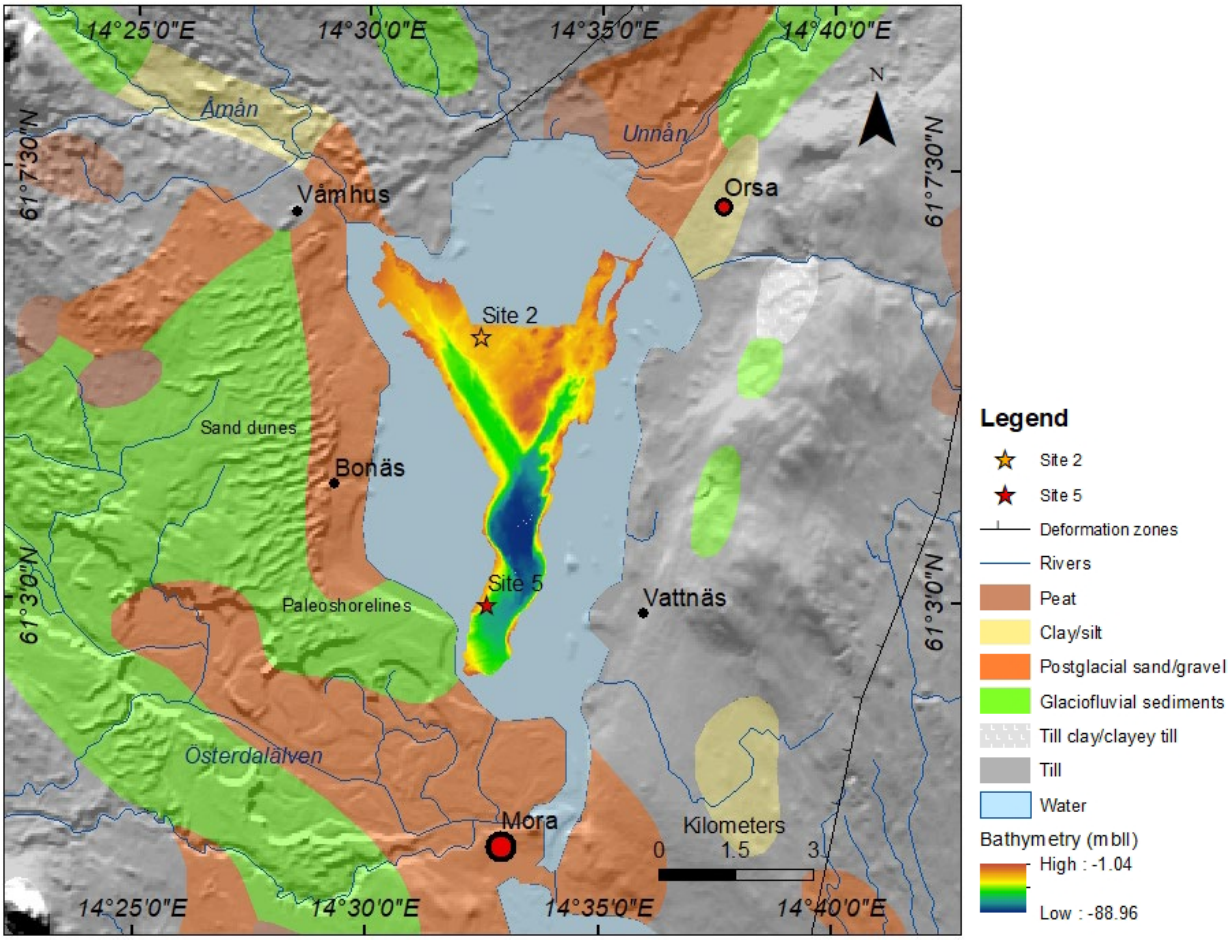

Figure 2: Map showing different soils, rivers, deformation zones and coring sites. Soil-map (Jordarter 1:1 miljon) and deformation zones (Berggrund 1:1 miljon) are provided from SGU and overlies a hillshaded DEM (GSD-höjddata, grid 50+) from Lantmäteriet. The river layer is provided from SMHI (flödeslinjer VD_1_2016_3). Bathymetry depths (meter below lake level, mbll) are referenced to the mean lake level, which is located 162 m above RH2000. Coordinate system SWEREF99_TM. The map is produced in ArcMap by Emelie Ståhl.

preconditions for the extensive glacial and glaciofluvial accumulations found around Lake Orsa. Glacial till covers much of the bedrock both at higher and lower altitudes, whereas glaciofluvial deposits are located mainly in the valleys at lower altitudes (Fig. 2). Wind, water, and the action of waves have subsequently reworked the sediments to various degrees. Glacial and glaciofluvial deposits have formed different types of moraines, eskers, and various of other landforms observable in the landscape (Nordell, 1984).

3. Material and methods

3.1. Echo sounding and backscatter principles

Mapping the seafloor with an incredible detail has become possible over the last decades, much thanks to the development of multibeam echo sounding (MBES) together with high-accuracy GPS positioning (Weber&Lurton, 2015; Jakobsson et al., 2016). With the introduction of multibeam sonar backscatter and angular range analyses it has also become possible to remotely characterize seafloor properties (Fonseca&Mayer, 2007).

3.1.1. Multibeam mapping

All echosounders basically function the same way; they generate and transmit a soundpulse (ping) towards the seafloor, and then measures the time-delay and intensity of the returned echo at a controlled angle of arrival (Lurton, 2002; Weber&Lurton, 2015; Jakobsson et al., 2016). The time-delay, or two-way-traveltime (TWT), can be converted to depth (*d*) if the sound velocity (*v*) is known using:

$$d = \frac{v\ x\ TWT}{2} \quad (1)$$

Correct sound velocity profiles are thus necessary for correct depth measurements. In multibeam surveys a good sound velocity profile is of fundamental importance, since sound beams at oblique angles will be refracted when they travel through layers with acoustic impedance contrasts arising from sound speed and density variations due to temperature and salinity fluctuations. A good sound velocity profile is needed to ray-trace the trajectory of the beam, which is necessary for calculating the correct depth (Lurton, 2002; Jakobsson et al., 2016). Correct depth measurements are also highly dependent on precise determination and compensation for the ships motion (heave, pitch, roll and yaw). An incorrect sound-velocity profile or inadequate motion compensation will generate different types of artefacts, which can be hard and time-consuming to remove during post-processing (Jakobsson et al., 2016).

Understanding a multibeam system´s resolution is a fundamental aspect when planning a survey. Horizontal resolution is defined as the smallest distance by which two features must be separated to be recorded as distinct objects. Equations 1 to 5 described below are from Jakobsson et al. (2016). The resolution of the multibeam sonar is depending on both the footprint diameter (D_f) and the first Fresnel zone. Since the first Fresnel zone is frequency-dependent, the footprint will generally determine the horizontal resolution in shallow water surveys when using high-frequency multibeam sonar systems (Martin Jakobsson, personal communication). The footprint diameter can be estimated based on the water depth (*H*) under the transducer and the opening angle (α) using:

$$D_f = 2H\ x\ \tan(\frac{\alpha}{2}) \quad (2)$$

The horizontal resolution of the sub-bottom profiler (SBP) is primarily depending on the first Fresnel zone (R_F). This is because a SBP mainly records the direct reflection and not the backscatter. The first Fresnel zone is the area where the reflected waves interfere constructively with the seafloor. This occurs when the acoustic soundwave is offset by up to one quarter of a wavelength (λ). Together with the water depth *(H)* the first Fresnel zone can be calculated using:

$$R_F \approx \sqrt{\frac{H\lambda}{2}} \quad (3)$$

The wavelength is directly proportionate to the velocity (*v)* and inversely proportionate to the frequency *(f),* and can be calculated using:

$$\lambda = \frac{v}{f} \quad (4)$$

Since the wavelength is inversely proportionate to the frequency, a higher frequency will give a smaller wavelength, which will generate higher resolution. However, higher frequencies are more easily absorbed in water, as the mechanical energy in the form of a soundwave will convert to heat, and thus high resolution must be traded against range of propagation (Lurton, 2002; Jakobsson et al., 2016). The operating frequency must thus be selected to give highest resolution possible while ensuring that the soundwave will be able to propagate to the seafloor and back, in the given water depth for the specific

survey. The vertical resolution (R_v) of the chirp sonar (a common type of SBP which is used in this survey) can be estimated based on the sound velocity and the bandwidth (*B*) using the Rayleigh criterion:

$$R_v \approx \frac{v}{Bx2} \quad (5)$$

The bandwidth is the same as the difference between the highest and lowest frequency limits of the outgoing acoustic signal (Jakobsson et al., 2016).

3.1.2. Backscatter and ARA

The amplitude of the returned echo, or the backscatter strength, is highly dependent on the angle of incidence and the difference in acoustic impedance between the water and the type of seafloor (Fonseca&Mayer, 2007; Lurton&Lamarche, 2015). The backscatter response from a hard material is higher than for a soft one, and a rough surface scatters more acoustic energy than a smooth surface. A rough and hard seafloor will scatter the sound waves almost equally in all directions, and the backscatter strength will depend only little on the incidence angle. The intensity recorded over the swath width from a rough and hard seafloor will thus be rather stable whatever the angle. A soft and smooth sediment sends back a maximum intensity at nadir, and only little at oblique angles. The sonar image will thus show a strong maximum at the vertical, and a fast decrease at the sides (Fig. 3) (Lurton&Lamarche, 2015).

To be able to create an easily interpretable backscatter image, the variations in intensity due to the incidence angle must be averaged out, so that a geologically homogenous seafloor appears at a constant level on the processed image, whatever the incidence angle. If preserved, the angular dependence of the backscattered response can be a powerful tool for seafloor classification. The method to analyse the angular dependence of the backscattered response is commonly referred to as angular range analysis, or ARA (Fonseca&Mayer, 2007; Parnum&Gavrilov, 2011) and is thoroughly described by Fonseca and Mayer (2007).

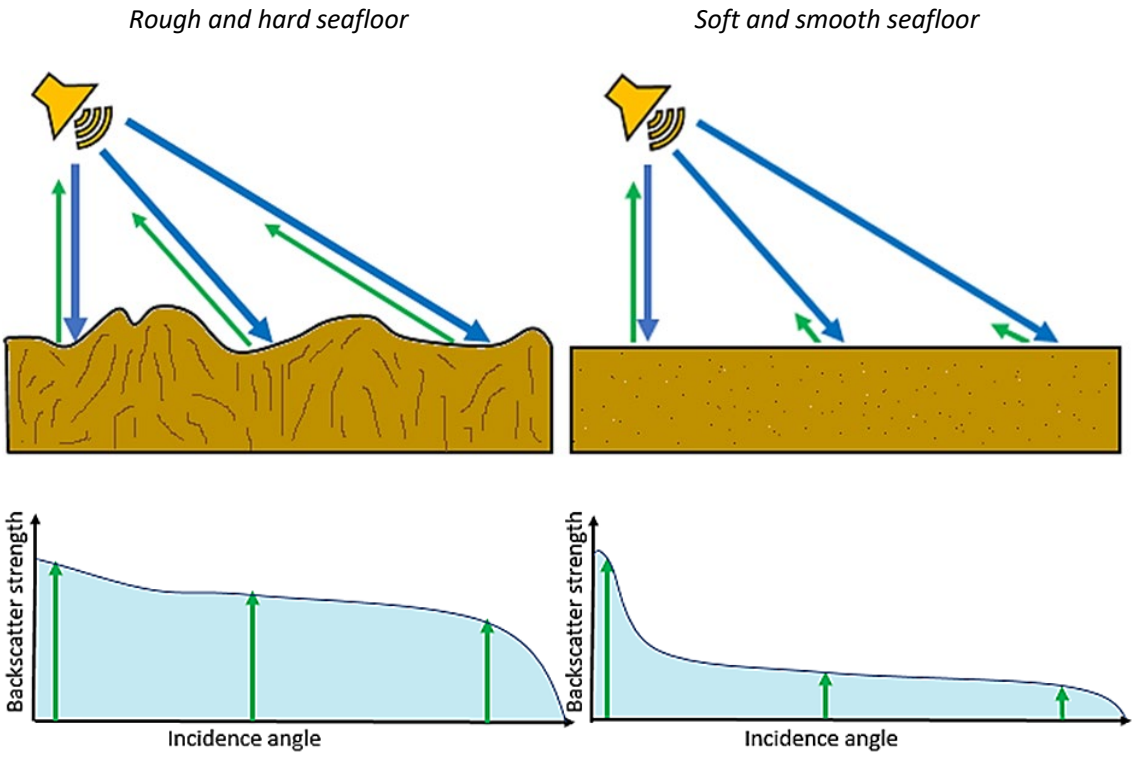

Figure 3: The figure illustrates the backscatter strength depending on incidence angle and different seafloor properties. Modified after Lurton&Lamarche, 2015.

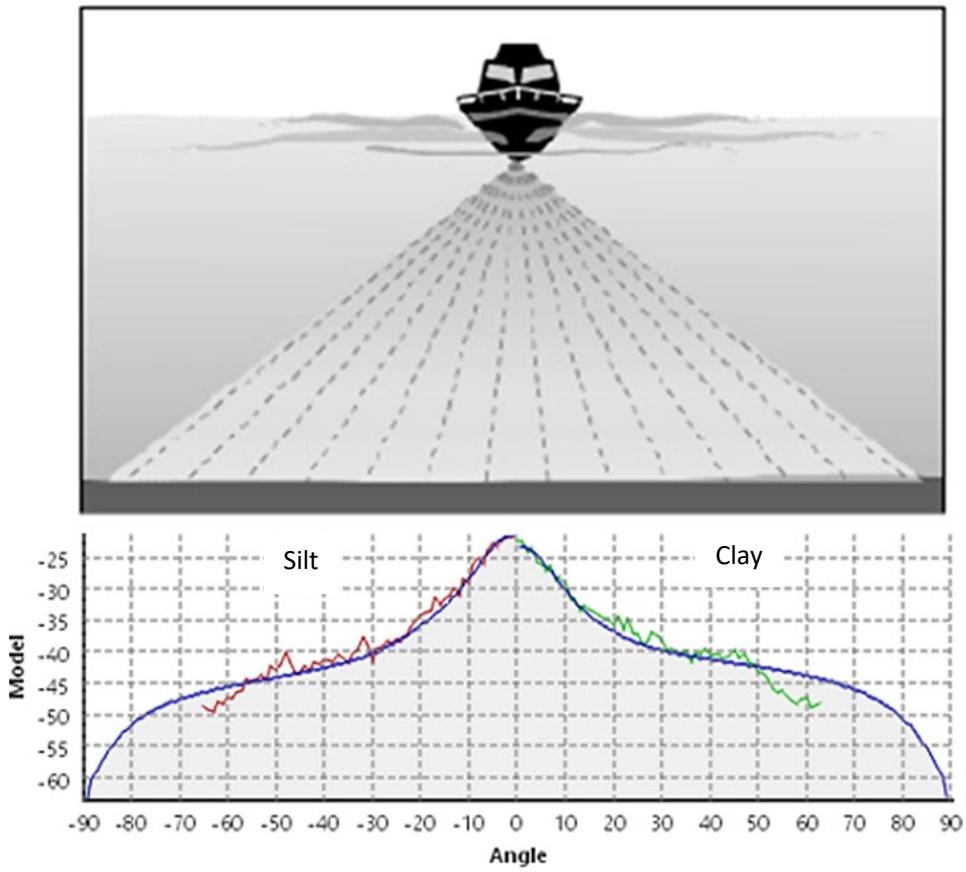

Figure 4: The figure illustrates how the model used in ARA estimates the character of the seafloor based on remotely acquired backscatter strength. The model is visualized as the blue line. The red saw-toothed line is the backscatter response from the port side of the research vessel, and the green line from the starboard side. Modified after Lurton&Lamarche, 2015.

ARA uses a mathematical model that links acoustic and physical properties (grain size, acoustic impedance, roughness) of known seafloor types to the backscattered response. The model is then used to inversely estimate the properties of the surveyed seafloor based on the remotely acquired backscatter (Fig. 4) (Fonseca&Mayer, 2007). Together with backscatter strength, ARA have proved to be the most useful backscatter characteristic for determining seafloor properties (Parnum&Gavrilov, 2011).

3.2. Field work

MBES bathymetry and backscatter characteristics have been used to map the bottom morphology and the physical and geological properties of Lake Orsa floor. Backscatter does not directly identify the bottom sediments, implying that in order to be able to classify the seafloor some kind of ground-truth information is needed (Parnum&Gavrilov, 2011). Drill cores provide information of the sediments at two sites in Lake Orsa. A sub-bottom profiler was also used to investigate the upper sedimentary stratigraphy.

3.2.1. Multibeam and backscatter measurements

Approximately 14 km^2 of multibeam data was acquired using a Kongsberg Maritime EM2040 0.7° x 0.7°, bow-mounted on Stockholm Universitys 6.4 m long survey boat *RV Skidbladner*. The MBES was operating with maximum ping rate (i.e. round trip) at a frequency of 300 kHz, apart from a few lines that were acquired at 400 kHz. A Seapath 320+ navigation system with MR5+ and RTK was used, improving the positioning accuracy to only a couple of centimetres. Sound velocity profiles were acquired using a Valeport miniSVP.

3.2.2. Sub-bottom profiling

Sub-bottom profiles where acquired using a Kongsberg EA640 Single Beam Echo sounder with an Air15-17 transducer, installed and deployed in a surface towed device custom made at the Department of Geological Sciences. The Air15-17 transducer has an optimal centre frequency of 15 kHz. The system was operating in chirp-mode with a pulse length of 1.024 ms and a bandwidth between 13-17 kHz.

3.2.3. Sediment coring

Sediment cores were acquired in April 2019 at two of five planned sites (Sites 2 and 5). The core at Site 2 was retrieved in the northern part of the lake at 61°5'45.13" N and 14°32'25.62" E (Fig. 2). Coring was stopped at a sub-bottom depth of 810 cm. The core at Site 5 was obtained in the posterior part of landslide 1 in the southern end of the lake at 61°2'57.88" N and 14°32'34.55" E (Fig. 2). Coring at site 5 reached a depth of 1148 cm. Only brief information from the cores regarding surface and sub-bottom sediments are included in this work as they are processed and analysed at Lund University. This information is used to calibrate the interpretation of the geophysical mapping data.

3.3. Post-processing

Processing of the MBES data was carried out in Qimera v1.7.3, a hydrographic sonar data processing software made by the company QPS. However, the data set was already rather clean as they were partly processed already during the field work and only minor additional postprocessing was needed. A final bathymetric surface with 1m cell-size was imported and further analysed in Fledermaus. Backscatter mosaic, statistics, and ARA were produced in Fledermaus GeoCoder Toolbox (FMGT) v7.8.5.40, also a software by QPS. Sub-bottom profiles were processed using the open-source program SegyJP2 by the Geological Survey of Canada, which converts SEGY files to (and from) the SGYJP2 format, which is needed to visualize the sub-bottom profile images in the accompanying program SegyJP2Viewer. Additional visualization and analyses including hillshading, slope analysis, as well as area and volume calculations were carried out in ArcMap v10.4.1. See Figure 5 below for workflow.

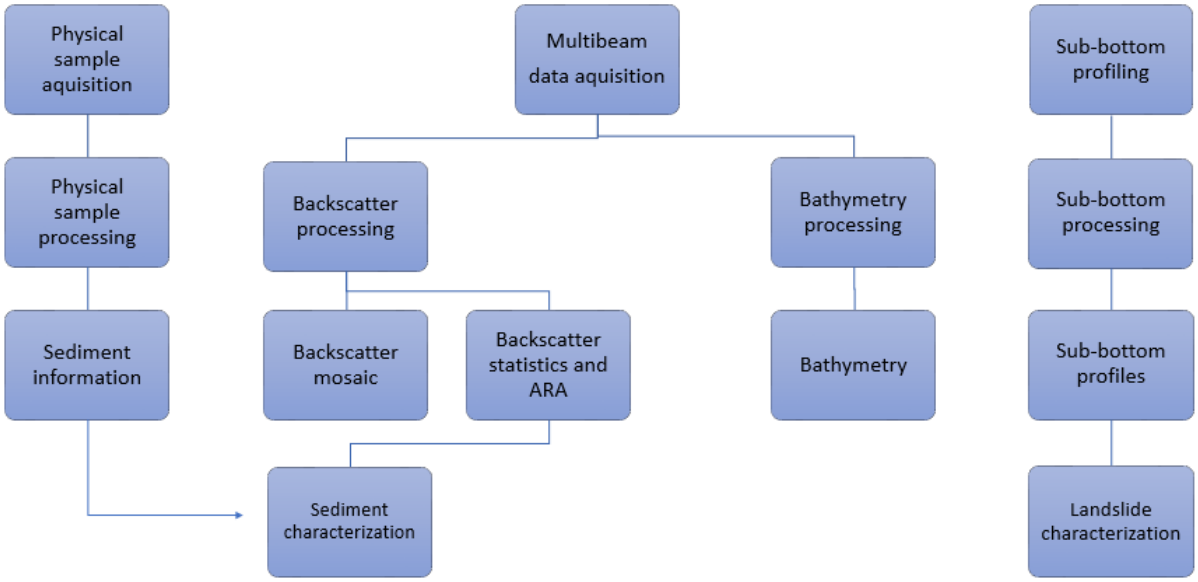

Figure 5: Illustration of workflow. Additional visualization and analyses have also been made in ArcMap.

3.4. Volume calculations

A conservative estimate of volume displaced sediment was generated based on point depth values from the sub-bottom profiles. The point depth values were imported to ArcScene and interpolated using the algorithm Natural Neighbour. The resulting raster showed a continuous surface representing the base of the slide. To be able to calculate the volume, the raster had to be converted to a triangular irregular network (TIN), after which a surface difference could be calculated with the surface bathymetry as reference layer.

4. Results

4.1. Quantitative characterization of submarine landslides

There is no standardized method for data collecting and characterization of submarine landslides, and thus the quantitative metrics, and how they are defined, varies between studies. This limits the possibility for comparison analyses between studies. In this study a simplified method proposed by Clare et al. (2018) has been used. Definition of slide dimensions are outlined in Figure 6.

Other limitations arise due to lack of data coverage. This problem is more pronounced with the sub-bottom profiles, as sub-bottom data were not gathered from all of the lake, and available data coverage from the landslides are scarce. The reason for not acquiring sub-bottom profiles along with the multibeam bathymetry is interference between the two systems (M. Jakobsson personal communication).

The accuracy of the quantitative measurements is depending on resolution of the geophysical mapping data. Smaller landslides require higher resolution to be measured more precisely. For example, the length of a complex feature, such as the length of a scarp perimeter, will increase if data resolution is enhanced (Clare et al., 2018). In this study a cell size of 1 m is used in the produced bathymetry, based on the MBES footprint of less than 1.10 m. This is sufficient to make good measurements considering the scale of the submarine landslides in Lake Orsa. Similarly, the resolution of the SBP is of equally importance when estimating the accuracy of the sub-bottom profile measurements (Clare et al., 2018). In this study the SBP has a vertical resolution of ~0.19 m. The thickness of the submarine landslides in Lake Orsa are generally less than 10 m, thus the accuracy for the quantitative measurements will not be as good as for the bathymetry measurements from the MBES.

At last, but not less important, there is a high degree of subjectivity in the interpretation of submarine landslides. The more complex the measured feature is, the greater degree of variability there will be between measurements from different researchers (Clare et al., 2018).

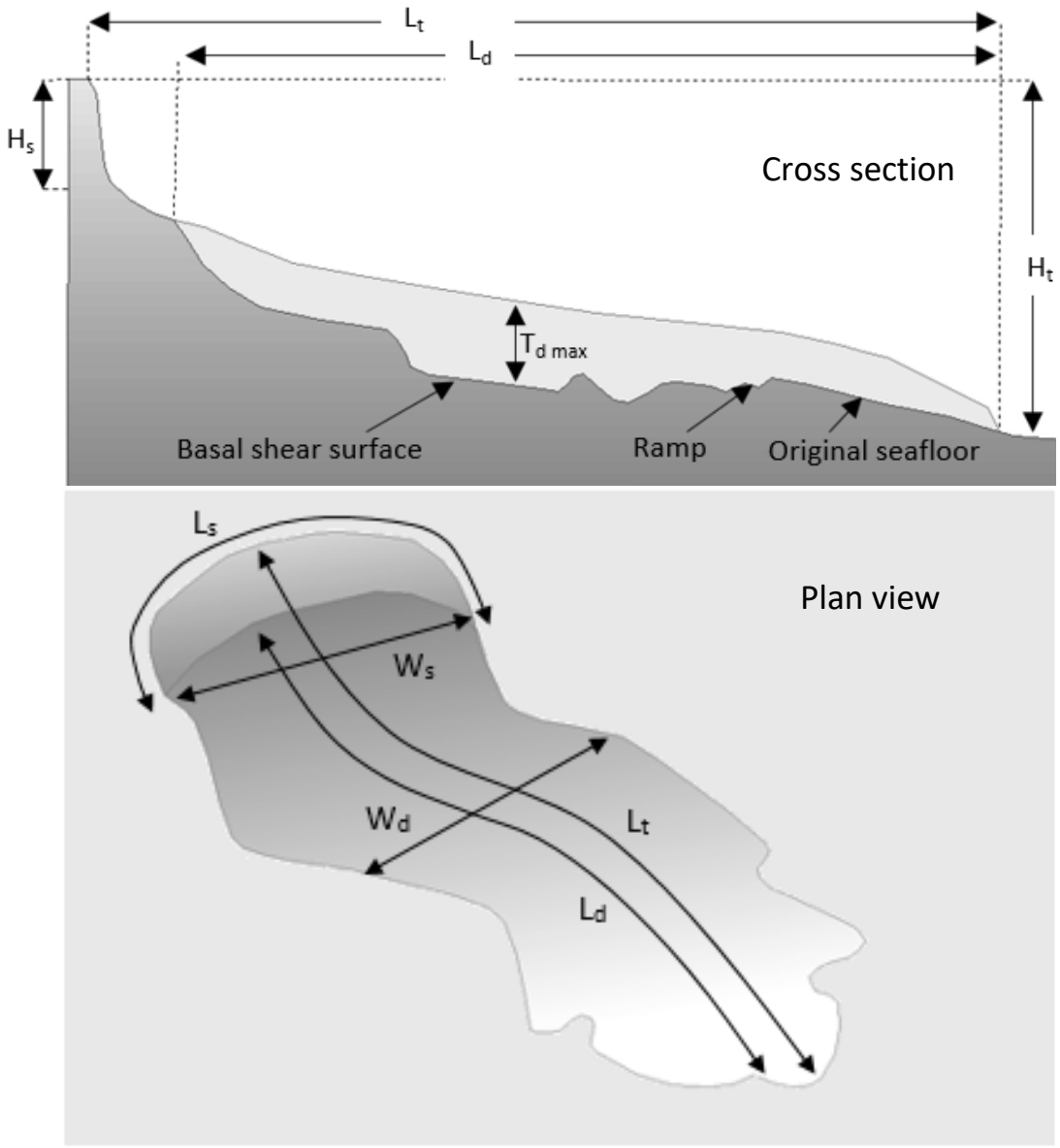

Figure 6: Schematic illustration of the defined and measured dimensions of the slides: H_s = Scarp height, L_t = Total length, L_d = Deposit length, H_t = Total height drop, T_{dmax} = Maximum deposit thickness, L_s = Scarp perimeter length, W_s = Maximum scarp width, W_d = Maximum mappable width (perpendicular to L_d). The landslide is an example of a frontally unconfined landslide.

4.2. Bathymetry

A total area of 13 768 600 m^2 was covered by the multibeam. The maximum depth in the surveyed area is 90 m, which is 4 meters shallower than the value provided by SMHI. The mean depth of the surveyed area is 39.54 m. An opening angle of 0.7° results in a maximum resolution of ~1.1 m according to equation 2, but if considering the mean depth, an average resolution of around 0.5 m can be expected.

Evidence of at least five submarine landslides are found within the study area, which hereafter are referred to as SL1, SL2, SL3, SL4 and SL5, see Figure 7 for location of the respective landslide. All landslides are found in the mid to southernmost part of the lake, and four of the five slides are located on the eastern lakeside. SL5 is an evacuated landslide scar without landslide debris. SL2 is the largest landslide and has an approximate total length of 635 m and is over 600 m wide (Table 1).

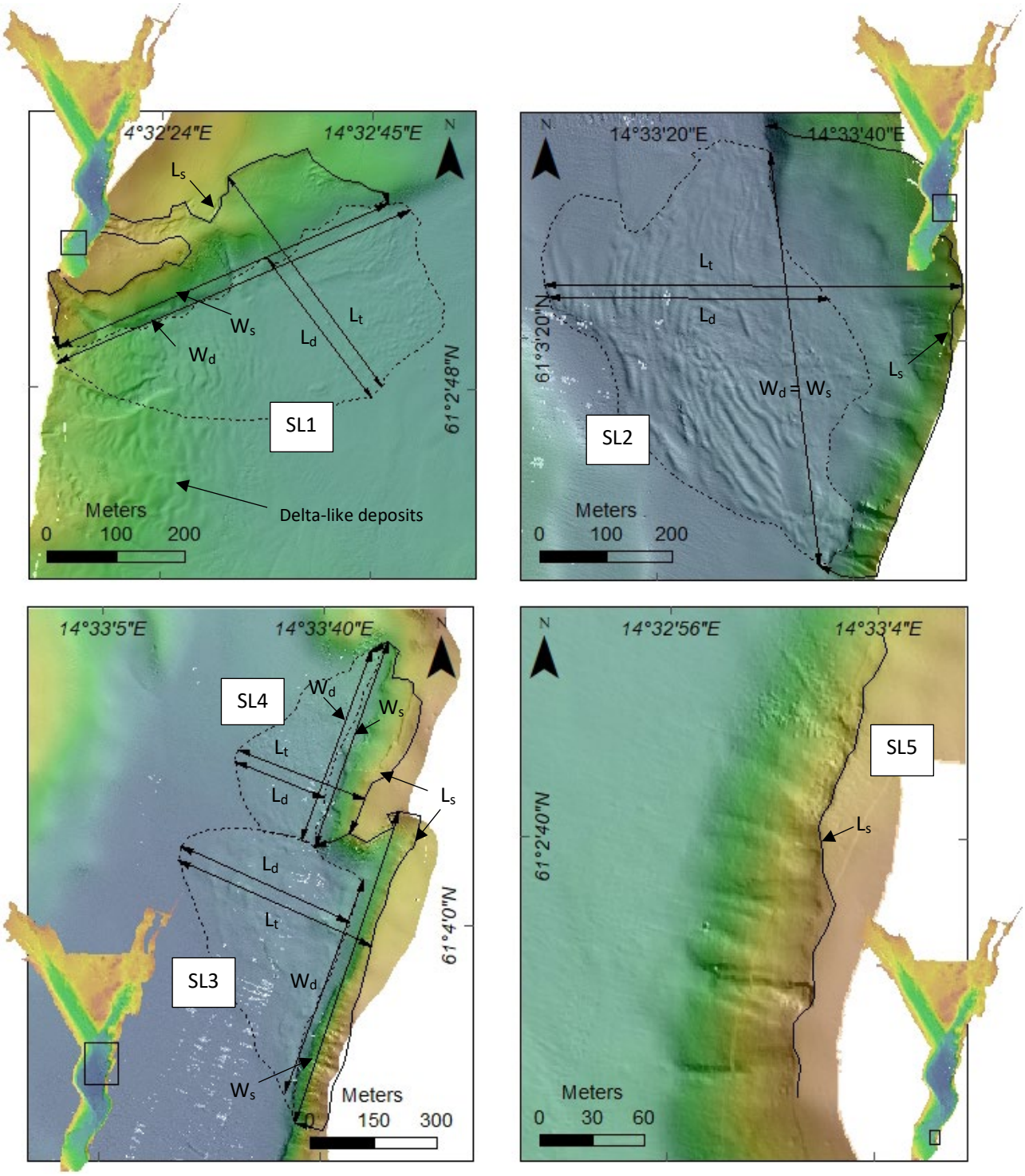

Figure 7: Location of the submarine landslides SL1 – SL5 in Lake Orsa along with measured dimensions. See Figure 6 for explanations of the defined dimensions and table 1 for measured values.

In addition to the submarine landslides, other morphological features can be seen. The higher parts of the lakefloor host several semi-circular depressions, similar in appearance to pockmarks, varying in size between approximately 10 to 70 m in diameter and with a general depth of 2 – 2.5 m. They are particularly abundant in the upper, central part of the lake (Fig. 8a). Erosional features of unknown origin can also be seen (Fig. 8b). In the top left part of the lake, a NW to SE trending sinusoidal feature approximately 2650 m in length, 60 to 80 m wide, and up to 3.5 m high is observed (Fig. 8c). Figure 8d shows the location of the described subaqueous landforms.

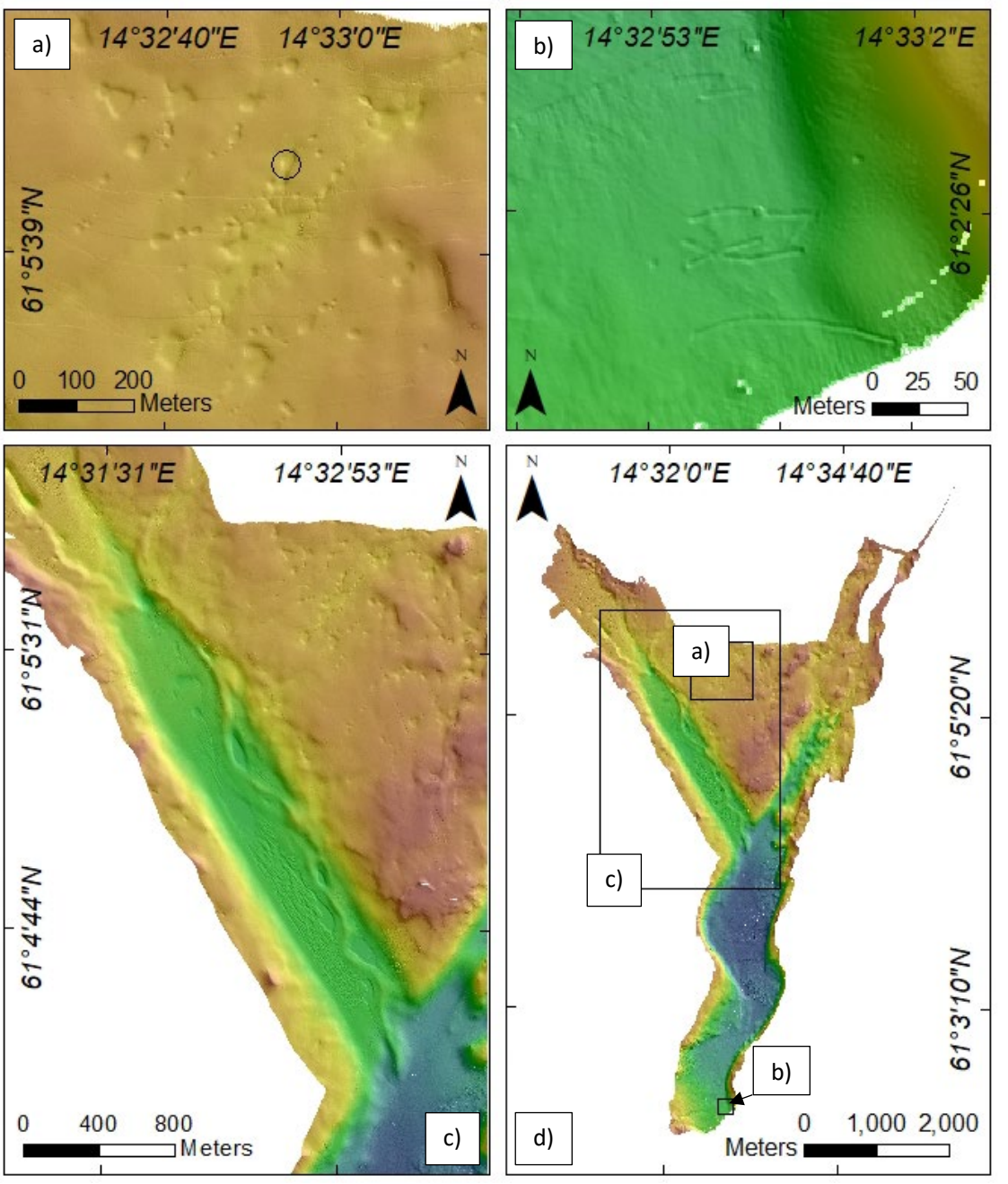

Figure 8: Various morphological features found at Orsa lake floor: a) Pockmark-like features from the upper, central part of the lake. The "pockmark" marked with a circle is seen in the sub-bottom profile in Figure 11a. b) Linear erosional features of unknown origin. c) A NW to SE trending sinusoidal feature approximately 2.7 km long. d) Location of the morphological features seen in a-c.

4.2.1. Mosaic and ARA

The produced mosaic shows a high backscatter strength response around SL1. The shallow north-eastern part of the lake has also generated a high backscatter response, but further to the west around the location for coring site 2, the response is again rather low. The backscatter strength is also low around SL2-SL5 (Fig. 9). The ARA suggests that the lakefloor mainly consists of clay and fine sand, but even gravelly sand is found in a few locations. The coarser sediments are mainly distributed towards the sides and at the higher parts of the lake, whereas clay dominate in the deeper sections. The ARA suggests that the deposit surface of SL1 consists of fine sand and medium to gravelly muddy sand. SL2-SL5 have deposit surfaces consisting of clay to fine sand (Fig. 10). The locations for the coarser sediments correspond to the locations with high backscatter strength in Figure 9. As mentioned before, results from ARA must be verified by some kind of ground-truth information. The physical descriptions (see further down) from the cores retrieved at site 2 and site 5 compare well with the ARA results.

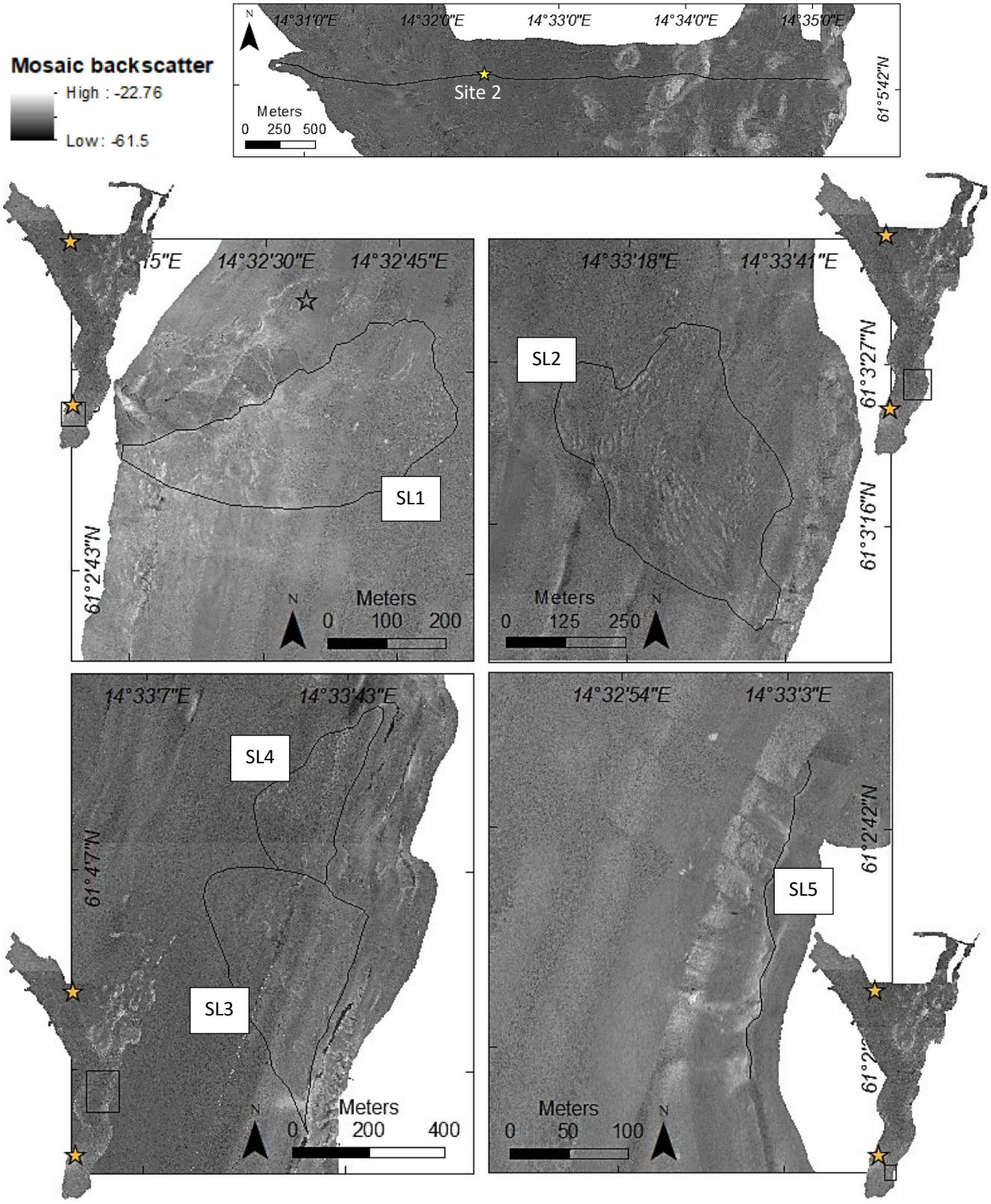

Figure 9: Produced mosaic from multibeam backscatter in Lake Orsa. Coring sites are marked with a star. The top figure has zoomed in on the survey track line (black line) for SBP1 (see below for explanation) and coring site 2. The rest of the figures are zoomed in on SL1-SL5.

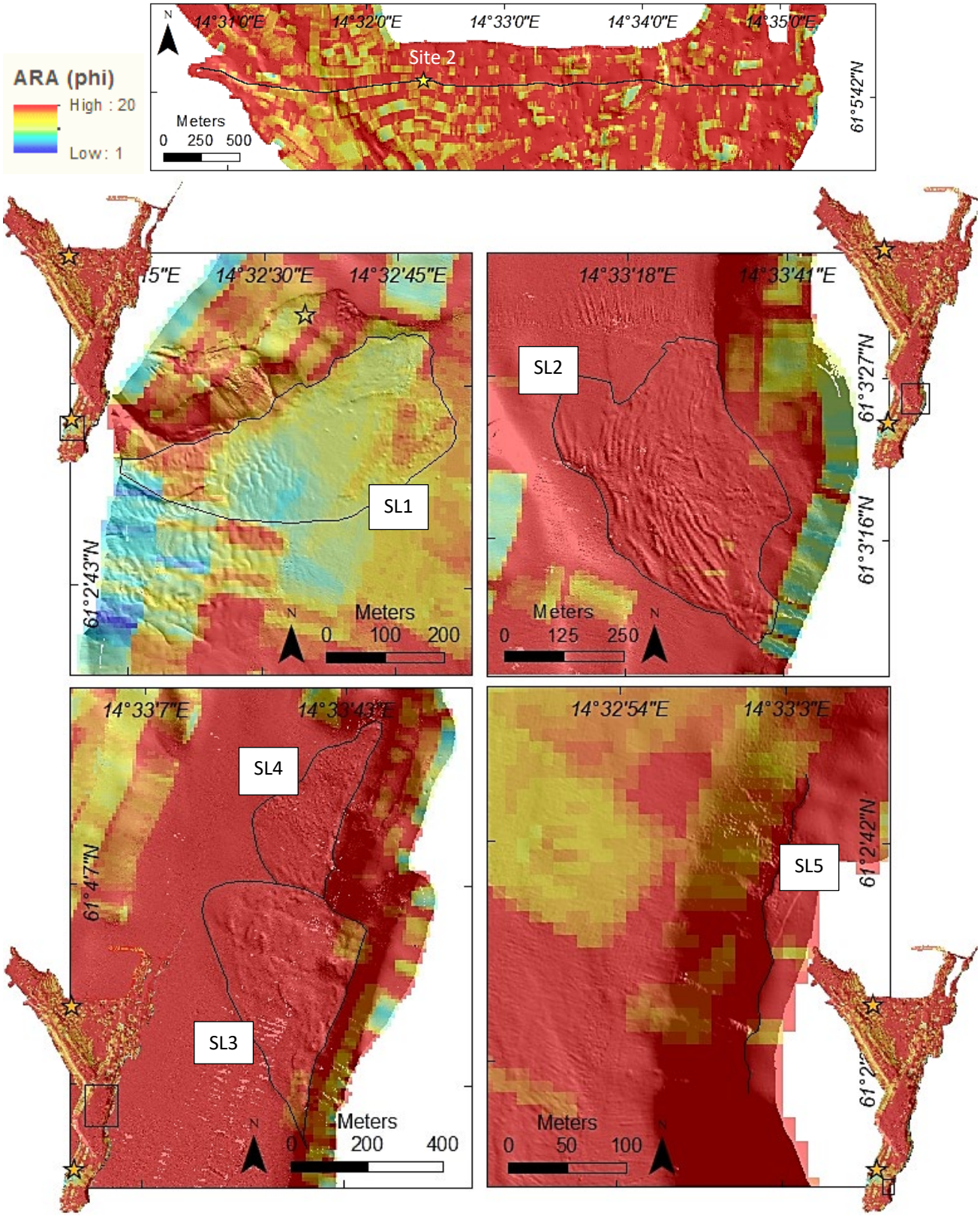

Figure 10: Produced ARA seafloor characterization based on the multibeam backscatter from Lake Orsa. The top figure has zoomed in on the survey track line (black line) for SBP1 (see below for explanation) and coring site 2. The rest of the figures are zoomed in on SL1-SL5.

4.3. Sub-bottom profiles

A frequency of 15 kHz and an approximate sound velocity of 1500 m/s give a wavelength of 0.1 m according to equation 4. A wavelength of 0.1 m and a maximum depth of 90 m gives a horizontal resolution of ~2.1 m according to equation 3, but considering the mean depth of 39.54 m a resolution close to ~1.4 m can be expected. A frequency limit between 13 and 17 kHz generates a vertical resolution of ~0.2 m according to equation 5.

The produced sub-bottom profiles are named SBP1, SBP2, SBP3 and SBP4 (Fig. 11a-c). The location for their respective survey track line can be seen in Figure 11d. An acoustic undisturbed sedimentary sequence is found at coring site 2 in SBP1 (Fig. 11a). These sediments are characterized by an acoustic stratified unit with an approximate thickness of 6 ms (TWT), which corresponds to ~4.5 m according to equation 1. Below this unit is a 3.2 m (TWT ~4.2 ms) thick stratified unit with low acoustic impedance found. The two units are separated by a distinct reflector (R1) caused by the strong impedance contrast between the two (Fig. 12).

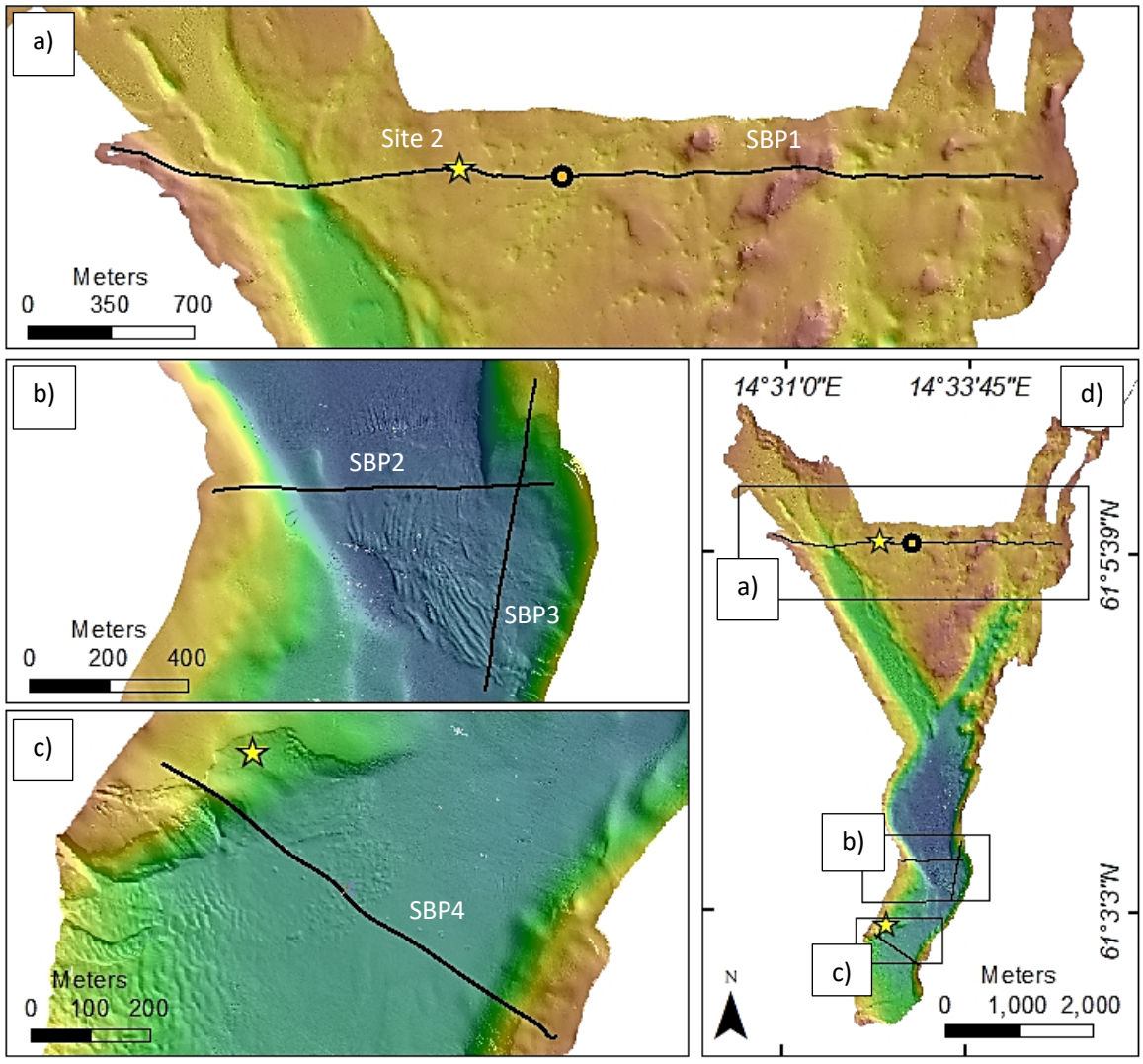

Figure 11: Survey track locations (black lines) a) SBP1 b) SBP3 and SBP4 c) SBP5 d) Location map. Coring sites are marked with a star, and the location of a pockmark-like feature is marked with a circle. This is the same "pockmark" marked with a circle in Figure 8a.

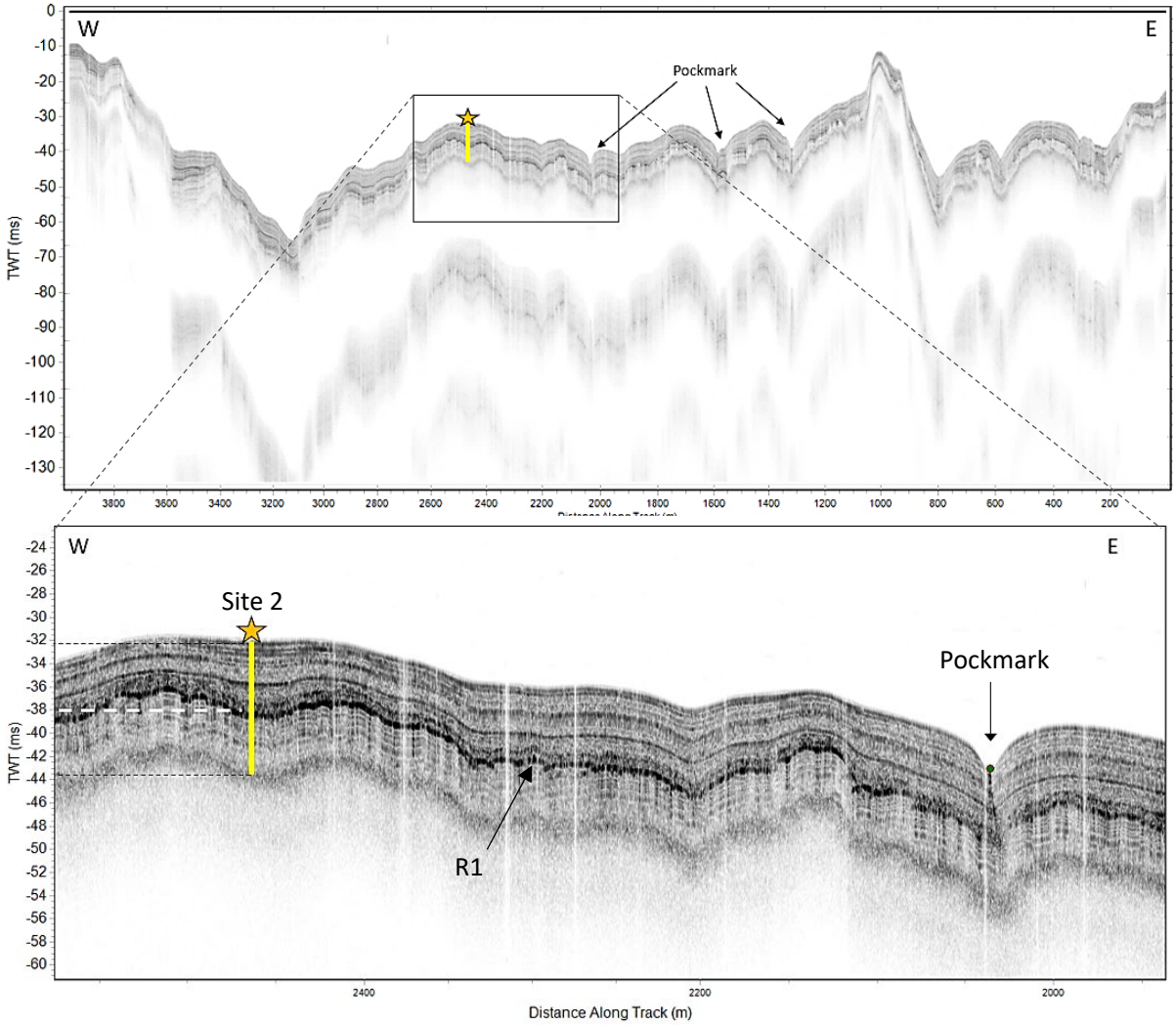

Figure 12: The upper sediments around coring site 2 in SBP1 are characterized by an acoustic stratified unit with a TWT of ~6 ms. R1 separates this unit from a 4.2 ms thick stratified unit with lower impedance below. The yellow line represents the retrieved core and is 8.10 m long.

The submarine landslides visible in the multibeam bathymetry are also clearly seen in the sub-bottom profiles. SL1 has a maximum sediment thickness ($T_{d\,max}$) of approximately 3.8 m (Fig. 13, Table 1) and SL2 has a $T_{d\,max}$ of approximately 10.8 m (Fig. 15, Table 1). The displaced sediments originating from the submarine landslides are highly disturbed and of low impedance. A more detailed description and interpretation is provided further down.

Characterization has been made based on frontal emplacement according to definitions proposed by Frey-Martinez et al. (2005). They divided submarine landslides into two main types; frontally emergent and frontally confined. In the former the displaced material ramps out the basal shear surface and onto the original lake- or seafloor. In this type there is nothing constraining the sediments, and they can move considerable distances over the undeformed original seafloor. In the latter the sediment mass is buttressed against the frontal ramp and does not abandon the basal shear surface (Frey-Martinez et al., 2006). Based on these definitions SL1 (Fig. 13) is characterized as a frontally emergent submarine landslide, and SL2 (Fig. 14) as a frontally confined. Unfortunately, there are no sub-bottom profiles from landslide 3 and 4.

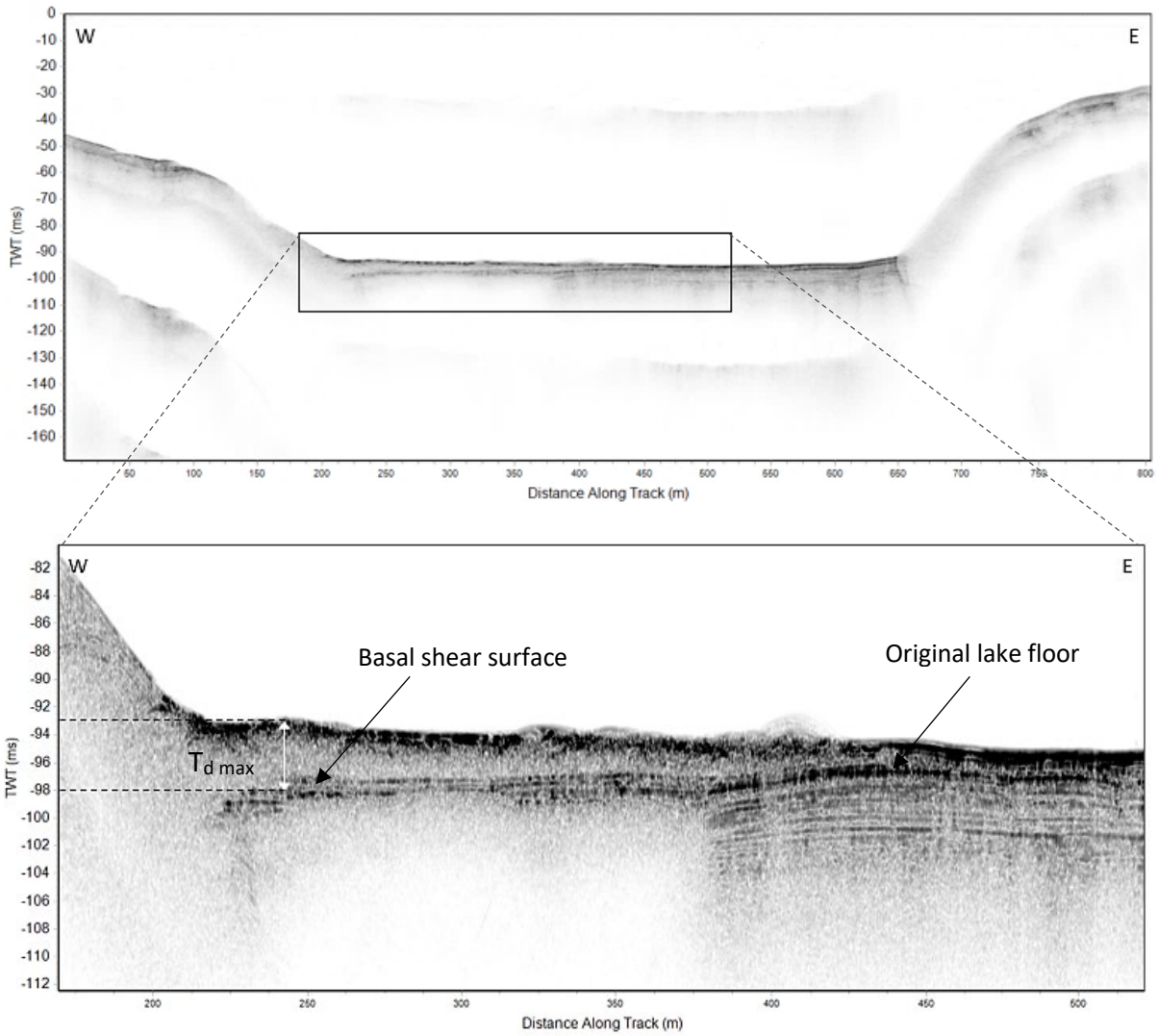

Figure 13: The displaced sediments in SL1 from SBP4 are highly disturbed and of low impedance. $T_{d\ max}$ is ~5 ms (TWT). The landslide front has left the basal shear surface and spreads out onto the original lake floor.

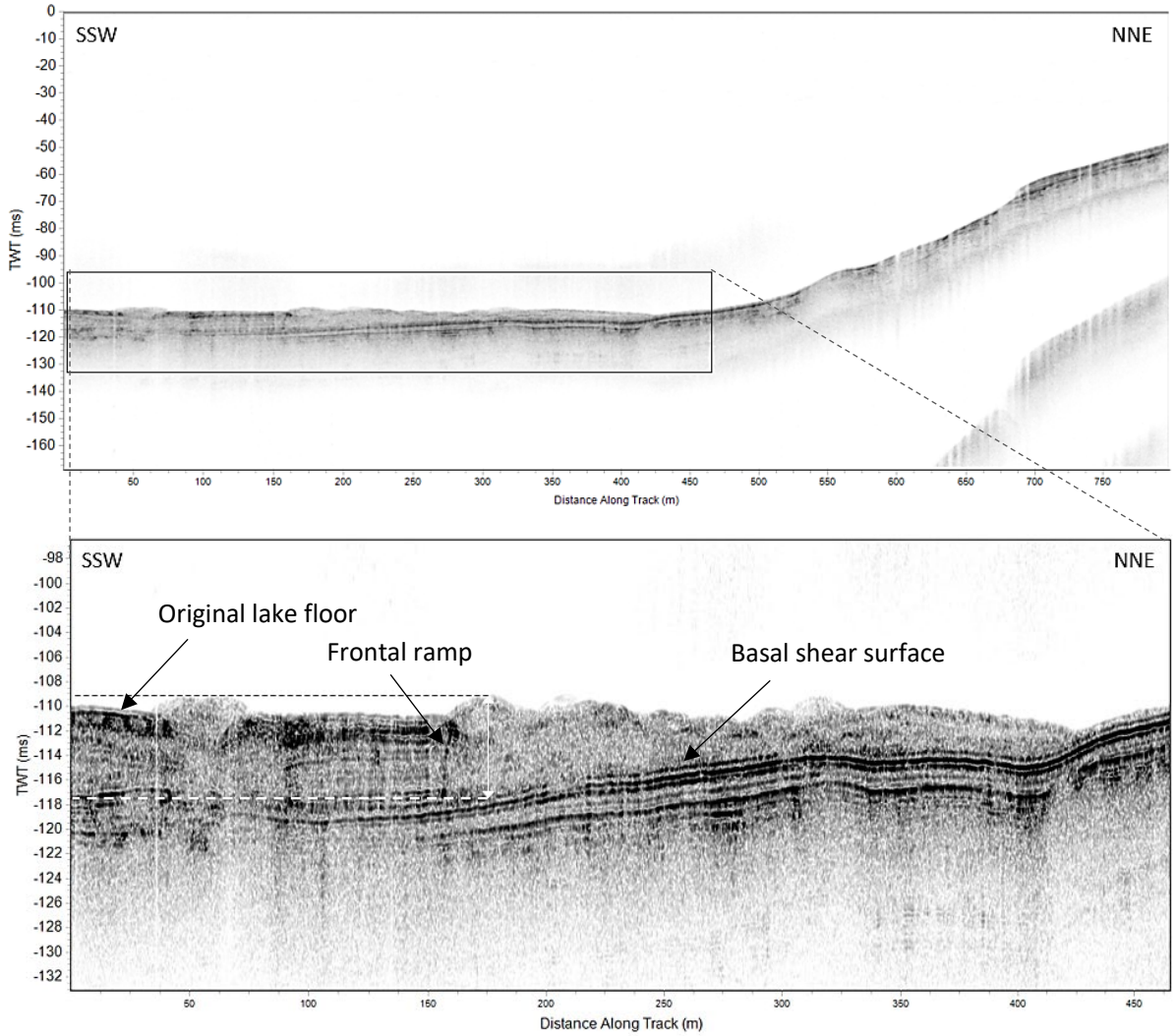

Figure 14: Highly disturbed sediments with low acoustic impedance is seen in SL2 (from SBP3). The front is buttressed against the frontal ramp and does not abandon the basal shear surface. The slide is thus characterized as a frontal confined landslide.

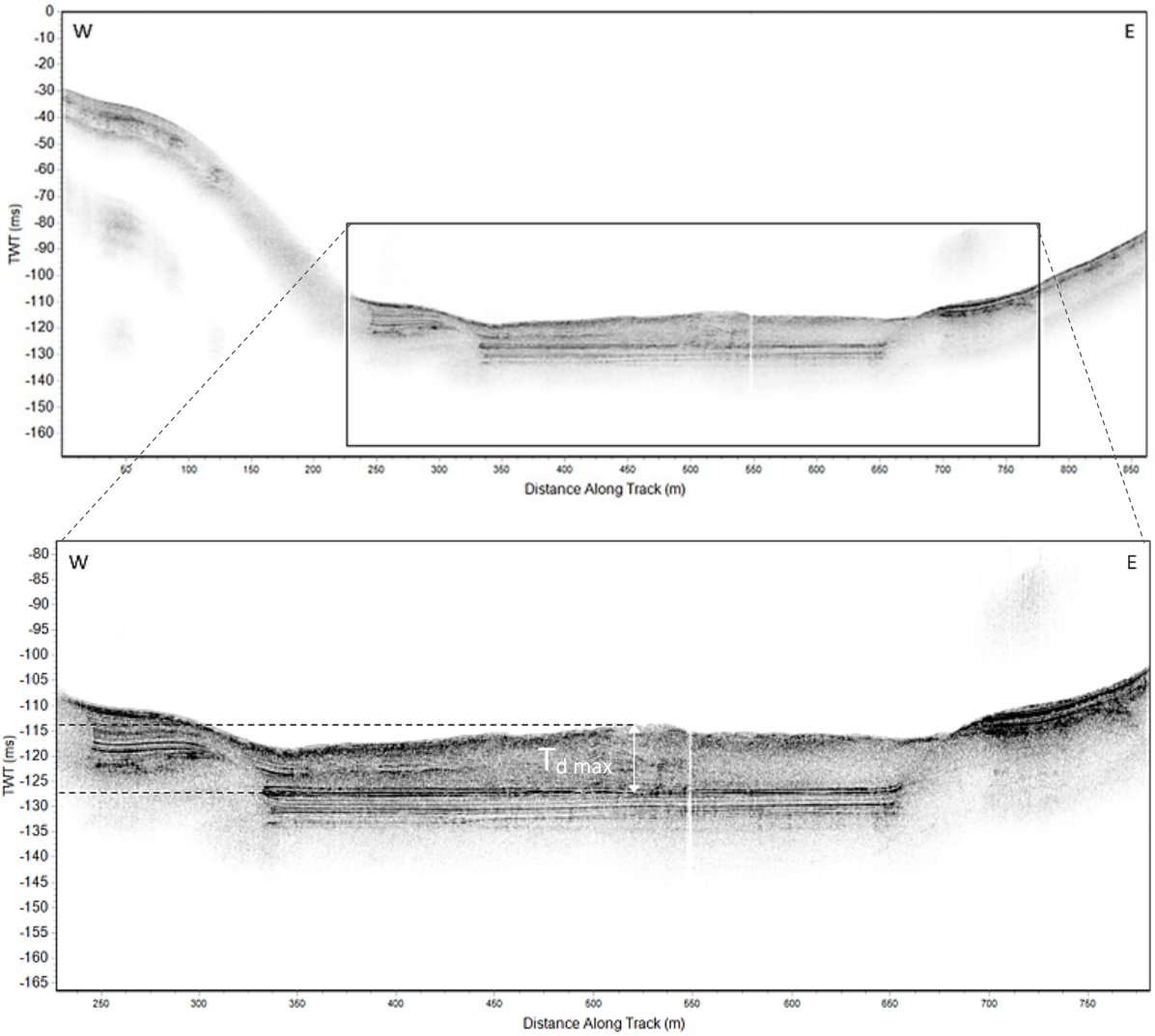

Figure 15: $T_{d\ max}$ in SL2 from SBP2 is ~14.4 ms (TWT). The disturbed sediment displaced from the slide has low acoustic impedance and lies on top of acoustic stratified sediment.

4.4. Sediment cores

The two cores retrieved from Lake Orsa have surface sediments consisting of laminated silty clay. The core at site 5 had yet not been opened and processed at the time for the writing of this report, but according to Per Möller (personal communication) the surface sediments in core 5 resembles the sediments from site 2. Visual results in the form of photographs were available from site 2, which is the base for following descriptions.

Two distinct sediment units occur in core 2. The upper unit consists of horizontal, finely laminated dark brown sediments interbedded with beige coloured laminations. The laminations range in thickness between a few mm up to a cm (Fig. 16a). The beige laminations increase in thickness with depth and get gradationally lighter in colour. At 3.88 meters below lake floor (mblf) the dark brown laminations terminate, which marks the transition to the lower sediment unit. This is a weakly layered section almost entirely consisting of light beige sediment (Fig. 16b). At approximately 5.50 mblf a disturbed sequence commences, which continuous throughout the rest of the core down to 8.10 m (Fig. 16c).

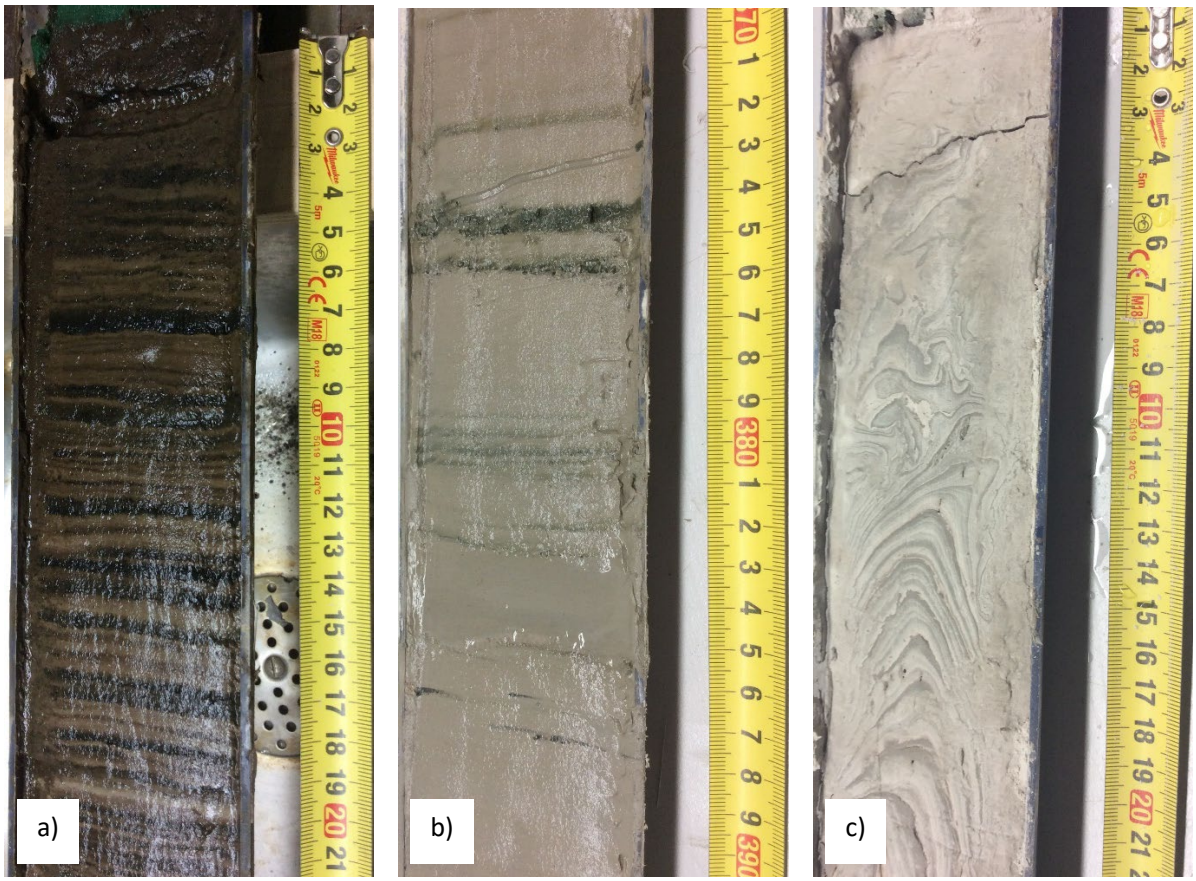

Figure 16: Selected sections of core at site 2.a) The uppermost section 0-0.21 mblf consisting of laminated silty clay gyttja. b) Location of the middle section at 3.70-3.90 mblf. Visualizes the termination of the dark-brown laminations at 3.88 mblf. c) This section is located 5.60-5.82 mblf and consists of a layered and disturbed unit.

4.5. Volume

A conservative estimate of volume displaced sediment contained in the largest submarine landslide (SL2) was estimated to approximately 6.2 x 10^5 m^3. A minimum sediment volume displaced by SL1 was assessed to 3.3 x 10^5 m^3 (Table 1).

Table 1: Table of measured values. D_{min} is the measured minimum depth of the landslide, and D_{max} the maximum depth, the other dimensions are defined in Fig. 6.

Landslide	SL1	SL2	SL3	SL4	SL5
L_t (m)	381	635	500	323	NA
L_d (m)	255	427	437	228	NA
L_s (m)	1100	1025	1185	619	NA
W_s (m)	525	631	781	517	NA
W_d (m)	561	631	538	480	NA
$H_{s\,max}$ (m)*	1.8	3	2.5	2.5	4
H_t (m)*	28	45	49.5	45	49
D_{min}* (mbll)	-40	-37.5	-36.5	-34	-15
D_{max}* (mbll)	-68	-82.5	-86	-79	-64
$T_{d\,max}$ (ms)**	5.0	14.4	NA	NA	NA
$T_{d\,max}$ (m)**	3.8	10.8	NA	NA	NA
Area (m^2)	99539	179218	153069	73517	NA
Volume (m^3)	336884	622336	NA	NA	NA
Slope (˚)**	10	25	30	17	22
Type	Frontally emergent	Frontally confined	NA	NA	Evacuated landslide scar
Surface sediment (ARA)	Fine and medium to gravelly muddy sand	Clay to fine sand	Clay to fine sand	Clay to fine sand	Clay to fine sand

Values not marked with an asterisk are measured in ArcMap
*Fledermaus
**Sub-bottom profiles

5. Interpretation and Discussion

The sinusoidal feature (Fig. 8c) is interpreted as an esker, a narrow sinusoidal ridge of sediment deposited by a meltwater stream, probably flowing through a tunnel within the glacier. When the glacier melted, the sediment was deposited onto the subglacial surface. The esker may suggest that an active ice-sheet was present in Vånådalen. The linear erosional features (Fig. 8b) are most likely anthropogenic in origin, maybe generated by dragging anchors.

Pockmarks have been described in the literature as the result of upward fluid- or gas flow (Jakobsson et al., 2016). The pockmark-like features in Lake Orsa (Fig. 8a) are not associated with the typical low impedance indicating flowing water or gas (which causes surface subsidence) nor are they associated with deformation and faulting of sediment typical for surface subsidence associated with a melted buried ice-mass (Boggs, 2014). They are thus thought to originate from the basement, maybe due to earlier glacial erosion, or maybe chemical dissolution (karstification), with the sediments draped on top.

There are no obvious signs to be able to visually relate the slides to the glacial landforms (i.e. the esker) and relating the slides to the postglacial evolution of the area is thus difficult. However, dating the

landslides will be possible once the retrieved sediment core during the drilling campaign in one of the slide deposits will be analysed.

The landslide deposits of SL5 are hardly seen on the multibeam bathymetry (SL5 in Fig. 7) nor on the sub-bottom profiles. It is thus interpreted as the oldest landslide since the displaced sediments likely have been eroded away. According to Nordell (1984), substantial sedimentation took place from Österdalälven when it discharged into the southwestern part of Lake Orsa. Palaeoshorelines after Österdalälven are clearly seen in Figure 2, and delta-like deposits suggesting river deposits can be seen in the bathymetry close to SL1 in Figure 7. SL1 has a younger sedimentary layer above the landslide deposit, which may indicate that this landslide has been present for a longer time and have had time enough to be covered by sediments. SL2 – SL4 lack a sedimentary cover on top of the displaced sediments, and do not carry any traces of notable erosion. They are thus interpreted as younger than SL1 and SL5. I thus propose that the landslides in Lake Orsa most likely are related to more than one single event.

Since the perimeter of the Siljan ring consists of Palaeozoic limestones and sandstones, the eroded material released from the melting ice-sheet is likely rich in carbonate. Highest concentrations in the lake sediments should be expected when the ice-sheet was close to the Lake, but as the ice-sheet receded further away, the concentrations most likely decreased as the ice-sheet would start to erode and pick up material from bedrock mainly consisting of granites. This might explain the gradual colour transition between the upper and the lower unit observed in the photographs from the core at site 2 (Fig. 16). The lowermost unit with low impedance is coloured in blue in Figure 17 and 18 and is believed to be the same unit. Based on previous reasoning, the core photographs (Fig. 16), and descriptions from Per Möller (personal communication), the lower unit is interpreted as carbonate-rich clay to silty clay deposited when the Ancylus lake was in close contact with the glacier margin. The acoustic stratification in the lower unit is thought to reflect general regular to semi-regular variations in grain-size and/or composition. This is consistent with the observed layering in the lower unit on the photographs from site 2 (Fig. 16c). The layering is likely varves formed in response to seasonal variations in meltwater flow and sediment supply. This is one of the most characteristic properties of glacial lakes (Boggs, 2014).

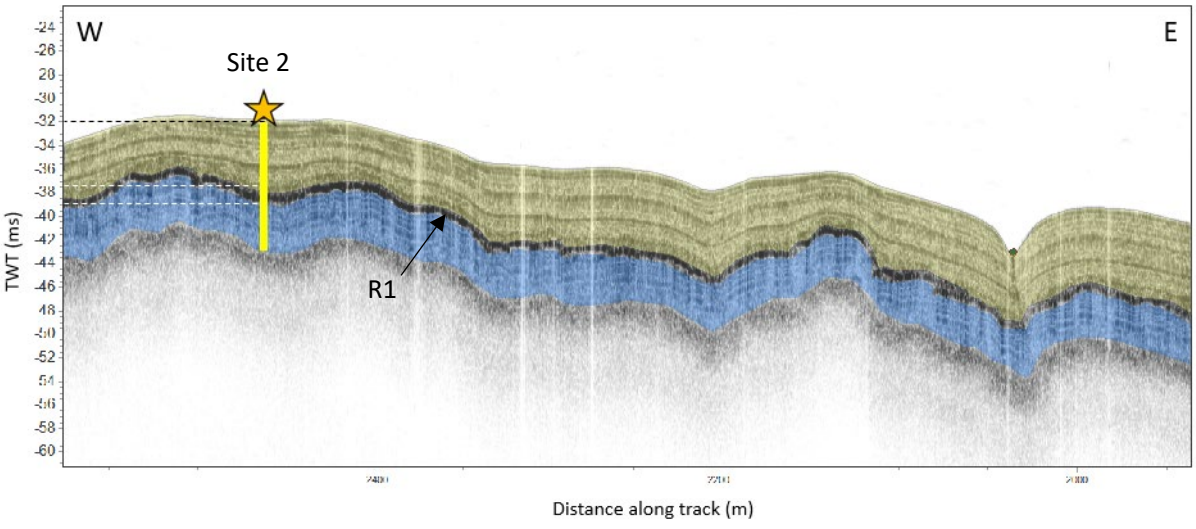

Figure 17: Interpreted sub-bottom profile from SBP1. R1 separates the acoustic stratified unit with high impedance coloured in yellow from the acoustic stratified unit with low impedance coloured in blue below.

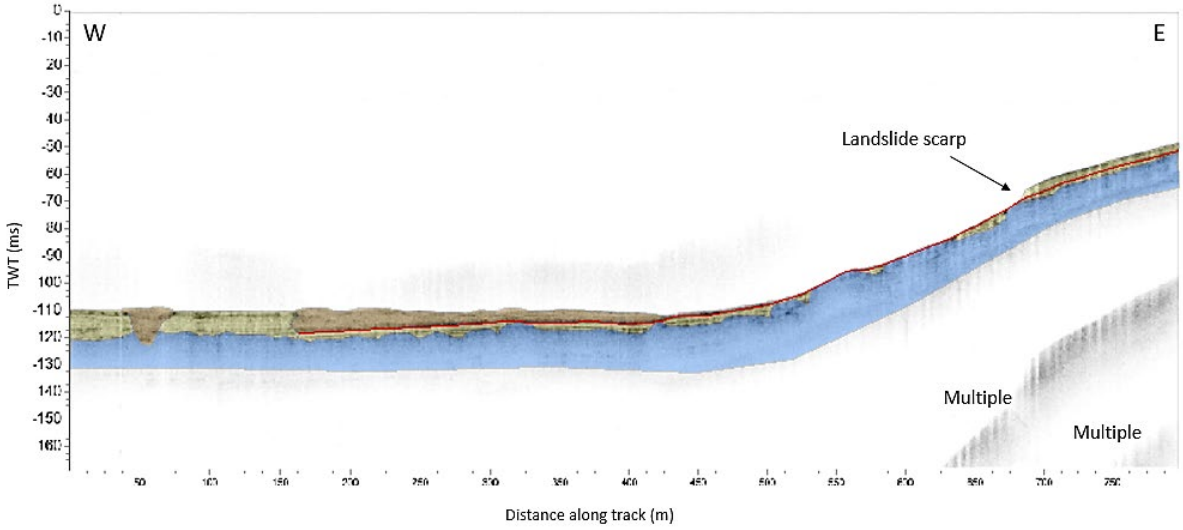

Figure 18: Interpreted sub-bottom profile from SBP3. The landslide debris is coloured in brown.

The upper acoustic stratified unit (coloured yellow in Fig. 17 and 18) is interpreted as fine-grained deposits (clay to silt) from an environment distal to the glacier. The climate was likely more habitable, and the dark brown laminations seen in the upper 4 m in core 2 (Fig. 16a,b) are likely layers with a high organic content. That the darker laminations in the upper 4 m arise from organic matter content is verified by Per Möller (personal communication). He suggests that the laminations may reflect variations in bottom oxygenation due to fluctuations in organic material, deposited during intermittent flooding-events during springtime. They may also originate from aquatic production during the summer. The absence of the dark brown laminations below 3.88 mblf is thought to reflect the cold and hostile climate when only minor production of organic material can be expected.

The interpreted sliding plane marked with a red line in Figure 18 is identified as a possibly low-strength layer which developed into a failure plane. Since the location between the upper and the lower units coloured in yellow and blue in Figure 17 and 19 coincides with R1, it is interpreted as the same plane responsible for generating the distinct reflector. This indicates that the two units have different sedimentological properties.

Models have showed that fast sedimentation rates can generate submarine landslides on continental slopes with a gradient as low as 2° (Talling et al., 2014). The slopes adjacent to the submarine landslides in Lake Orsa varies between 10° to 30° (Table 1). Steeper slopes are gravitationally less stable and require only small triggers to fail. The steep lake floor in Lake Orsa thus facilitated for the slope failure to occur. Excess pore pressure is a key factor for slope failure, and commonly develops if rapid deposition of low permeable sediments occurs. The terminus of glacial ice-streams is a typical surrounding where prolonged and rapid sedimentation occurs. Low permeability prevents fluid to dissipate along drainage paths, thus leading to excess pore pressure (Vanneste et al., 2012; Talling et al, 2014). Excessive pore pressures act to support the overburden, and a rise in pore pressure lowers the vertical effective stress, which in turn undermines the shear strength in the sediments leading to decreased slope stability. If the excessive pore pressure supports all of the overburden, the slope is at the point of failure (Fig. 19). I suggest that the upper unit high in gyttja and clay content prevented fluids to dissipate from the lower unit, thus creating highly water-saturated sediments and the build-up of excessive pore pressures.

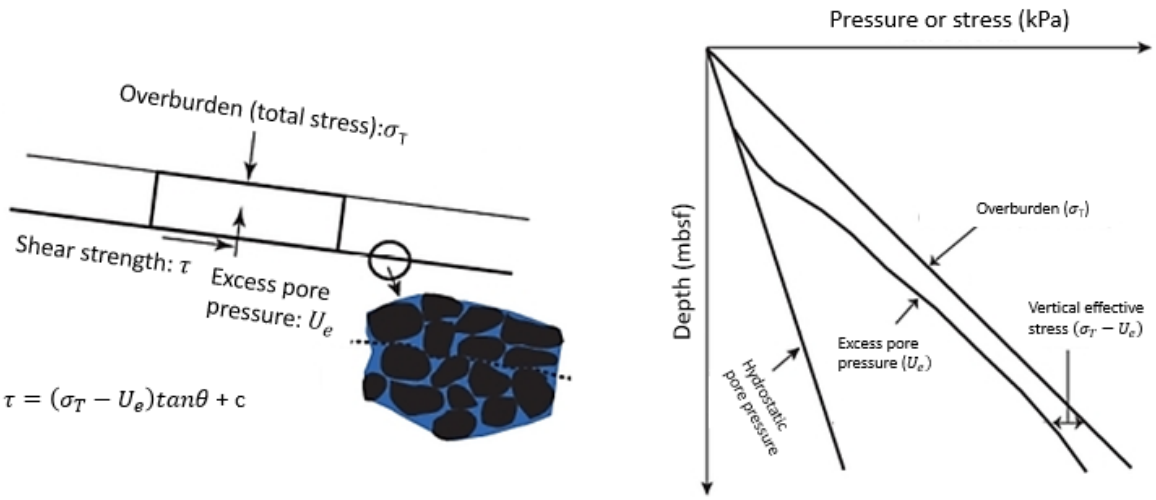

Figure 19: Illustration of the relation between shear strength (τ), total stress/overburden (σ_T), and excess pore pressure (U_e). Modified from Talling et al., 2014.

The palaeoshorelines seen in Figure 2 indicate that Lake Orsa may have been dammed by the Late Weichselian ice-sheet. Drainage of the ice-dammed Lake Orsa might have led to a rapid lake level fall. Sea/lake level rise or fall has also been linked to submarine landslides. It is here important to point out the difference between hydrostatic pore pressure within the sediments, and excess pore pressure. Hydrostatic pressure is the result from the weight of the overlying water column and acts equally in all directions. The sediments are thus not pressed down by the weight of the water column, and changes in hydrostatic pressure alone does not make a slope more likely to fail. However, sea or lake level fall has been linked to slope failures in shallow water. This might be explained by expansion of gas bubbles leading to elevated pore pressures (Talling et al., 2014).

Faulting along pre-existing astrobleme associated fracture zones due to glacio-isostatic rebound could have caused earthquakes. Earthquake(s) have been proposed to be responsible for the large landslides observed in Lake Vättern (Jakobsson et al., 2014), and is another plausible triggering factor responsible for the development of the landslides in Lake Orsa.

The Rissa landslide affected almost 20% off the lake floor (L`Heureux et al., 2012). The total area of the landslides in Lake Orsa is 52.32 km^2, and even if the landslides had happened all at once, their total area of 0.51 km^2 would still just affect less than 1% of the lake floor. I therefore find it unlikely that they, even if they were related to one single event, could have caused an inland tsunami of the size observed in Rissa. The mass movements observed in Finneidfjord are found where slope angles vary between 13° and 21°. The Finneidfjord landslide displaced 1 x 10^6 m^3 of sediment and left scarp heights between 2 to 3 m in height. The slide likely occurred on thin, laminated, and soft clay beds distinct to the normal homogenous post-glacial sediments. Likely triggering factors include a weak sedimentary unit, high Holocene sedimentation rates, steep flanks, and excess pore pressure development (Vanneste et al., 2012). The preconditions in Lake Orsa are not too unlike those that led to the 1996 Finneidfjord landslide, and due to the closely situated cities around Lake Orsa I think these newly revealed landslides should be further evaluated to be able to make a comprehensive risk assessment.

Conclusion

The landslides in Lake Orsa are thought to be of different age and are not believed to be related to one single event. The largest landslide in Lake Orsa mobilized more than 620 000 m^3 of sediment. The length of the displaced sediment reaches over 630 m and is over 400 m wide. A likely weak horizon is located between two units with different sedimentological properties, which have left a strong reflector observable in the sub-bottom profiles. Likely triggering factors are thought to be a combination of high sedimentation rates leading to overpressure zones, steep flanks, and a weak horizon that developed into a failure plane. Other factors as earthquakes and/or a rapid lake level fall are considered plausible. Relating the landslides to the postglacial evolution of the area will be possible once the results are available from the retrieved cores. A thorough risk assessment and evaluation for potential future slope failure to occur in Lake Orsa should be done in order to protect nearby citizens.

Acknowledgements

Firstly, I want to thank my supervisor professor Martin Jakobsson for all the help and guidance through this project. I am also very grateful to professor Per Möller and professor Dan Hammarlund at Lund University for letting me take part of the results from the sediment cores (although they had yet not been fully processed at the time for this report). At last, I will direct my full gratitude to my family, who has supported me and encouraged me throughout my studies, from the very start three years ago to the end with the writing of this report.

References

Björck, S. (1995). A Review of The History of The Baltic Sea, 13.0-8.0 ka BP. Quaternary International. 27, p19-40.

Boggs, S (2014). *Principles of Sedimentology and Stratigraphy* . 5th ed. Essex: Pearson Education. p237-245.

Clare, M., Chaytor, J., Dabson, O., Gamboa, D., Georgiopoulou, A., Eady, H., Hunt, J., Jackson, C., Katz, O., Krastel, S., León, R., Micallef, A., Moernaut, J., Moriconi, R., Moscardelli, L., Mueller, C., Normandeau, A., Patacci, M., Steventon, M., Urlaub, M., Völker, D., Wood, L., Jobe, Z (2018). A consistent global approach for the morphometric characterization of subaqueous landslides. *Geological Society, London, Special Publications*. 477.

Clarke, S., Hubble, T., Airey, D., Yu, P., Boyd, R., Keene, J., Exon, N., Gardner, J., and Shipboard Party SS12/200. (2012). Submarine Landslides on the Upper Southeast Australian Passive Continental Margin – Preliminary Findings. In: Yamada, Y., Kiichiro, K., Ikehara, K., Ogawa, Y., Urgeles, R., Mosher, D., Chaytor, J., Strasser, M *Submarine Mass Movements and Their Consequences, 5th International Symposium*. Springer. p55-66.

Fonseca, L., Mayer, L. (2007). Remote estimation of surficial seafloor properties through the application Angular Range Analysis to multibeam sonar data. *Marine Geophysical Research*. (28), p119-126.

Frey-Martinez, J., Cartwright, J., James, D. (2006). Frontally confined versus frontally emergent submarine landslides: A 3D seismic characterisation. *Marine and Petroleum Geology*. 23, p585-604.

Hampton, M.A., Lee, H.J. (1996). Submarine Landslides. *Reviews of Geophysics*. 34 (1), p33-59.

Henkel, H., Aro, S. (2005). Geophysical Investigations of The Siljan Impact Structure - A Short Review. In: Koeberl, C., Henkel, H *Impact Tectonics*. Heidelberg: Springer. p247-284.

Holm-Alwmark, S., Rae, A.S.P., Ferrière, L., Alwmark, C., Collins, G.S. (2017). Combining shock barometry with numerical modelling: Insights into complex crater formation—The example of the Siljan impact structure (Sweden). *Meteoritics & Planetary Science*. 52 (12), p2521–2549.

Jakobsson, M., Björck, S., O`Regan, M., Flodén, T., Greenwood, S.L., Swärd, H., Lif, A., Ampel, L., Koyi, H., Skelton, A. (2014). Major earthquake at the Pleistocene-Holocene transition in Lake Vättern, southern Sweden. *Geology*. 42 (5), p379-382.

Jakobsson, M., Gyllencreutz, R., Mayer, L.A., Dowdeswell, J.A., Canals, M., Todd, B.J., Dowdeswell, E.K., Hogan, K.A., Larter, R.D. (2016). Mapping submarine glacial landforms using acoustic methods. In: Dowdeswell, J.A., Canals, M., Jakobsson, M., Todd, B.J., Dowdeswell, E.K., Hogan, K.A. *Atlas of Submarine Glacial Landforms: Modern, Quaternary and Ancient*. Bath: The Geological Society. p17-40.

L'Heureux, J-S., Eilertsen, R.S., Glimsdal, S., Issler, D., Solberg, I-L., Harbitz, C.B. (2012). The 1978 Quick Clay Landslide at Rissa, Mid Norway: Subaqueous Morphology and Tsunami Simulations. In: Yamada, Y., Kiichiro, K., Ikehara, K., Ogawa, Y., Urgeles, R., Mosher, D., Chaytor, J., Strasser, M *Submarine Mass Movements and Their Consequences, 5th International Symposium*. Springer. p507-516.

L'Heureux, J-S., Longva, O., Steiner, A., Hansen, L., Vardy, M.E., Vanneste, M., Haflidason, H., Brendryen, J., Kvalstad, T.J., Forsberg, C.F., Chand, S., Kopf, A. (2012). Identification of Weak Layers and Their Role for the Stability of Slopes at Finneidfjord, Northern Norway. In: Yamada, Y., Kiichiro, K., Ikehara, K., Ogawa, Y., Urgeles, R., Mosher, D., Chaytor, J., Strasser, M. *Submarine Mass Movements and Their Consequences, 5th International Symposium*. Springer. p321-330.

Lurton, X (2002). *An Introduction to Underwater Acoustics, Principles and Applications*. Chichester: Praxis Publishing Ltd.

Lurton, X., Lamarche, G. (2015). Introduction to backscatter measurements by seafloor-mapping sonars. In: Lurton, X., Lamarche, G *Backscatter measurements by seafloor-mapping sonars Guidelines and Recommendations*. p11-24.

Mosher, D.C., Shimeld, J., Hutchinson, D., Lebedeva-Ivanova, N., Chapman, B.C. (2012). Submarine Landslides in Arctic Sedimentation: Canada Basin. In: Yamada, Y., Kiichiro, K., Ikehara, K., Ogawa, Y., Urgeles, R., Mosher, D., Chaytor, J., Strasser, M *Submarine Mass Movements and Their Consequences, 5th International Symposium*. Springer. p147-157.

Muhamad, H., Juhlin, C., Lehnert, O., Meinhold, G., Magnus Andersson, M., Juanatey, M.G., Malehmir, A. (2015). Analysis of borehole geophysical data from the Mora area of the Siljan Ring impact structure, central Sweden. *Journal of Applied Geophysics*. (115), p183-196.

Möller, P. (2005). Rogen moraine: an example of glacial reshaping of pre-existing landforms. *Quaternary Science Reviews*. 25, p363-389.

Nadim, F. (2012). Risk Assessment for Earthquake-Induced Submarine Slides. In: Yamada, Y., Kiichiro, K., Ikehara, K., Ogawa, Y., Urgeles, R., Mosher, D., Chaytor, J., Strasser, M *Submarine Mass Movements and Their Consequences, 5th International Symposium*. Springer. p15-27.

Nordell, P.O. (1984). Dokumentation av istida landformer, isavsmältning och högsta kustlinje i Våmådalen och Orsasjöns Randområden. *Information från Länsstyrelsen i Kopparbergs län, Naturvårdsenheten*. N 1984:4, pp72

Parnum, I.M., Gavrilov, A.N . (2011). High-frequency multibeam echo-sounder measurements of seafloor backscatter in shallow water: Part 2 – Mosaic production, analysis, and classification. *International Journal of the Society for Underwater Technology*. 30 (1), p13-26.

SMHI (2017). *Sjödjup och sjövolym (753kB.xlsx).* Available: https://www.smhi.se/klimatdata/hydrologi/svenskt-vattenarkiv. Last accessed 28th May 2019.

Talling, P.J., Clare, M., Urlaub, M., Pope, E., Hunt, J.E., Watt, S.F.L. (2014). Large Continental Submarine Landslides on Continental Slopes, Geohazards, Methane Release, and Climate Change. *Oceanogrophy*. 27 (2), p33-43.

Vanneste, M., L'Heureux, J-S, Baeten, N., Brendryen, J., Vardy, M.E., Steiner, A., Forsberg, C.F., Kvalstad, T.J., Laberg, J.S., Chand, S., Longva, O., Rise, L., Haflifason, H., Hjelstuen, B.O., Forwick, M., Morgan, E., Lecomte, I, Kopf, A., Vorren, T.O., Reichel, T. (2012). Shallow Landslides and Their Dynamics in Coastal and Deepwater Environments, Norwa. In: Yamada, Y., Kiichiro, K., Ikehara, K., Ogawa, Y., Urgeles, R., Mosher, D., Chaytor, J., Strasser, M *Submarine Mass Movements and Their Consequences, 5th International Symposium*. Springer. p29-41.

VISS, Vatteninformationssystem Sverige. *Orsasjön.* Available: https://viss.lansstyrelsen.se/Waters.aspx?waterMSCD=WA40066995. Last accessed 28th May 2019.

Weber, T., Lurton, X. (2015). Background and Fundamentals. In: Lurton, X., Lamarche, G *Backscatter measurements by seafloor-mapping sonars Guidelines and Recommendations*. p25-52.